Chapter 5

DATA PROCESSING

5-1 Introduction

The principal objective of the data processing was to provide corrections to the raw data of the airborne- and the experimental ground-radiometric surveys, and the laboratory gamma-ray spectrometric analysis of rock specimens collected from the study area.

The processing of the airborne radiometric data includes the basic reduction and signal enhancement. The basic reduction, which provides standard presentation of airborne radiometric maps, covers the selection of data of the study area from the data base, the re-positioning of co-ordinates of individual data point, the improvement of statistical adequacy to the data, the removal of background radiation, spectral stripping, and the normalization of altitude.
The enhancement of the signals primarily deals with the recovery of radiometric impulses from the spatially-filtered data. This process includes the computation of the inverse-filter coefficients from the spatial response of an infinitesimal radioactive point source situated on the ground surface, and the convolution of the inverse-filter coefficients with the recorded data. Radiometric maps of the enhanced data are also presented. Prior to the map-plotting works, further statistical analysis namely variography and variogram modelling (Balia,1983) were performed. These process were subsequently followed by the generation of the equally-spaced data mesh using the Kriging method (Balia,1983).

The correction of the experimental ground radiometric survey data includes the re-positioning of co-ordinates, the improvement of statistical adequacy to the data, the normalization of count rates, the removal of background radiation, the downward continuation of the normalized-and-background-removed count rates to the ground surface, spectral stripping, and the computation of concentration and ratios of concentration of each radioelement. The corrected data were presented in the form of profiles of radiometric parameters showing concentration of each radioelement.

The laboratory gamma-ray spectrometric analysis mainly concerns with polynomial curve fitting to evaluate spectral peaks of individual radioelement K, U, and Th, and calculate the abundance of uranium and thorium in rock specimens collected from the study area. High order (6th to 8th) polynomials were employed to provide the best fit to the spectral data.

The flow diagram of data processing of the airborne and the experimental ground radiometric surveys is shown in Figure 5.1. The schematic diagram of data processing of the laboratory gamma-ray spectrometry is presented in Figure 5.2.

Several computer programs have been written and adapted to perform the processing tasks on the DEC-2060 computer system, under the TOPS-20 Monitor 5.1(6101) operating system. All programs were written in FORTRAN-20 version 7 - based on the ANSI standard X3.9-1978. The 1022 Data Base System (Software House,1980) and the Minitab Statistics Package (Pennsylvania University,1981) were used for sorting and analysing the correlation coefficients of the airborne and the experimental ground radiometric data. The <PLOT79> Graphics Software Package (Beebe,1982) was used for creating the coloured maps. Annotation on the maps was done using the annotation-option of the MAP79 Contouring Package (Balia,1983). The IGS and PV Graphics Software (Creedy,1985) were used for creating radiometric profiles and plotting the coloured maps of the airborne radiometric data. The PV program facilitates plotting on various devices within the University's DEC-20R system environment. (The DEC-20R is a local configuration of a DEC-2060 intended for research purposes at the University of New England, Armidale).

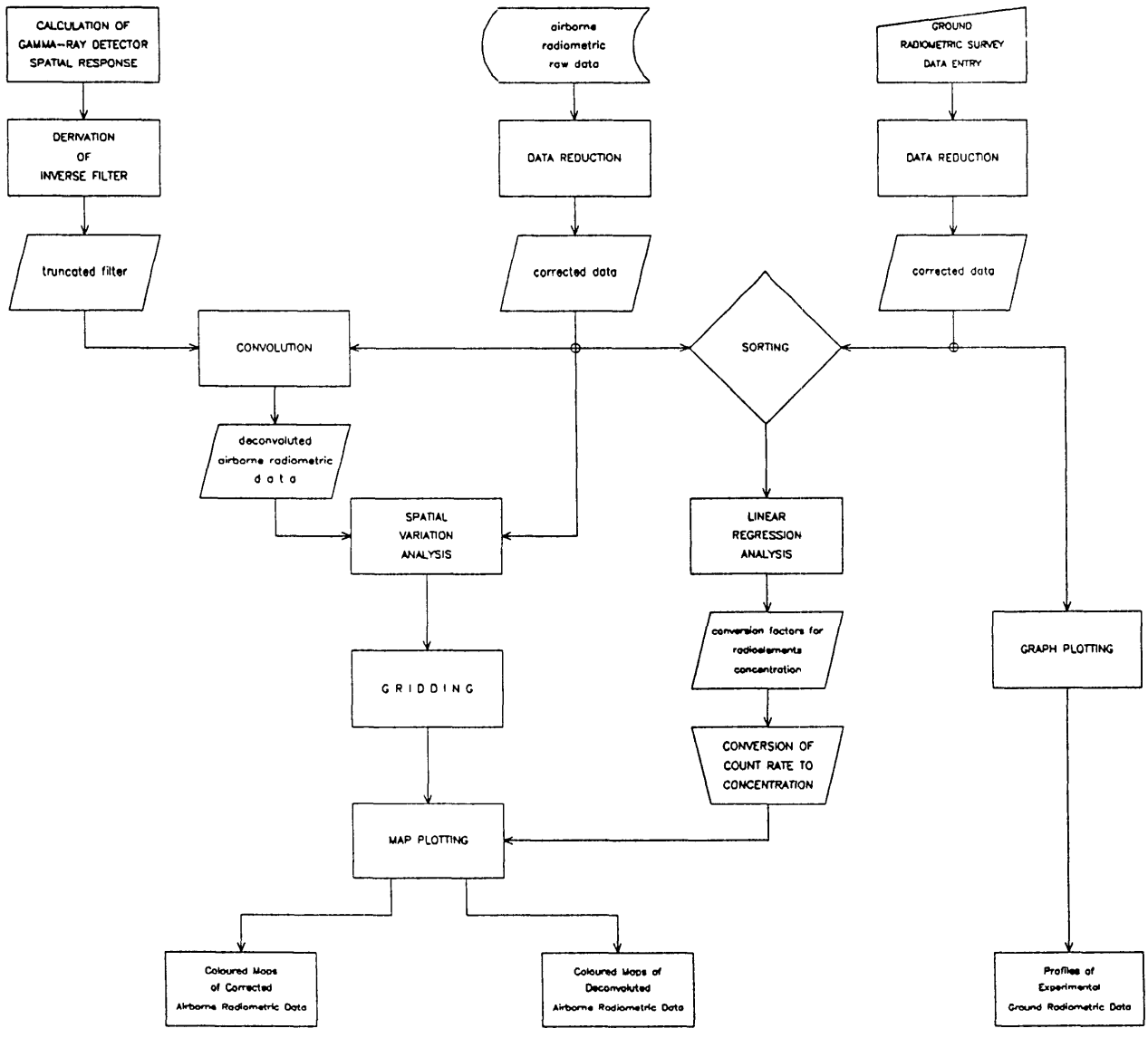

Figure 5.1 Flow diagram of data processing of the airborne and experimental ground radiometric surveys.

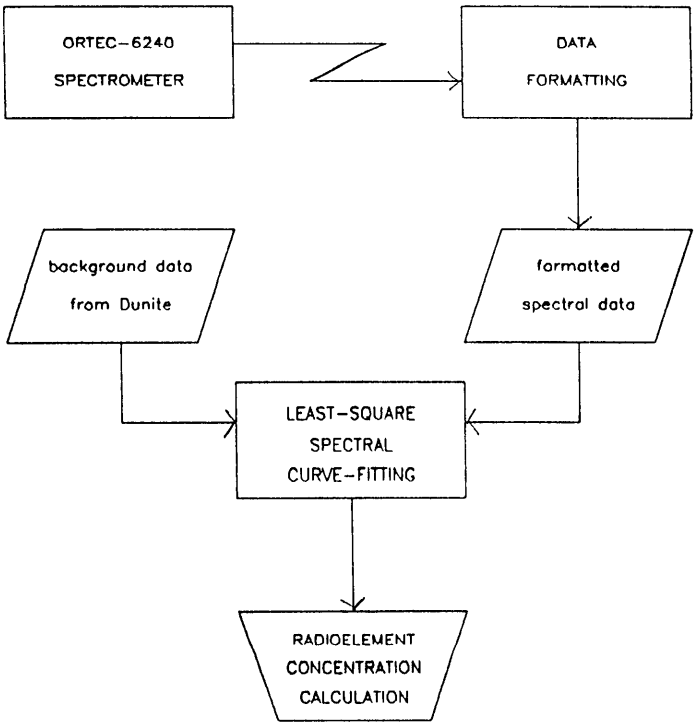

Figure 5.2 Flow diagram of data processing of the laboratory γ-ray spectrometric analysis of rock samples.

5-2 Data processing of the airborne radiometric survey

The data processing of the airborne radiometric survey includes :

- reduction of the airborne radiometric raw-data into corrected data;
- spatial variation analysis of corrected data;
- generate gridded data from the corrected data;
- conversion of normalized counts of corrected data into elemental concentration;
- plotting coloured maps of the corrected data;
- inverse-filtering of corrected airborne radiometric data;
- spatial variation analysis of the filtered data;
- generate gridded data from the filtered data;
- conversion of normalized counts of filtered data into elemental concentration;
- plotting coloured maps of the filtered data.

Reduction of the Airborne Radiometric Data

The reduction of the airborne radiometric data is implemented in the AIRAD computer program. Figure 5.3 shows the flow chart of the program.

Selection of the area

The reduction process was initiated by specifying the border co-ordinates which include the study area. The initially-selected area was 20% wider than the finally-mapped area. The 20% excess area width allows the kriging program, KRIG2D (Balia, 1983) to produce better gridding results at the margin of the finally-mapped area. Figure 5.4 shows the size of the finally-mapped area relative to the initially-selected area.

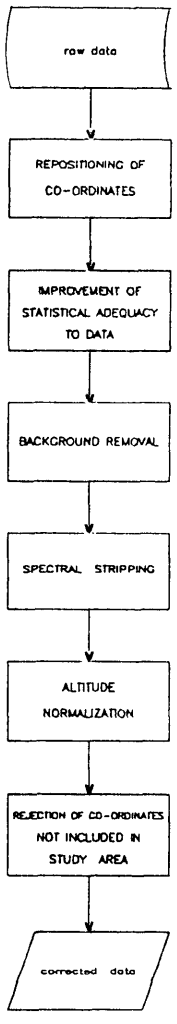

Figure 5.3 Flowchart of program AIRAD, used to perform reduction of the airborne radiometric data.

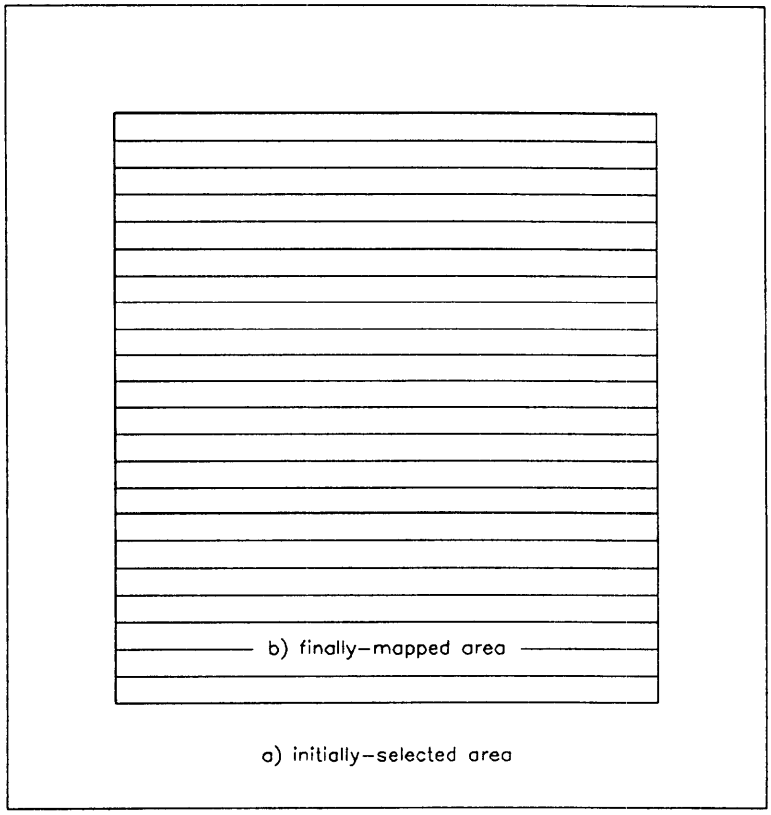

Figure 5.4 Relative sizes of the initially-selected and finally-mapped areas.

Co-ordinate translation

The next processing step performed translation of the co-ordinates of the data points. A new position of a data point lies between its previous position, when counting commenced, and the position of the next data point when counting of the next interval commenced. Thus, a centre point or a new co-ordinate is associated with a value accumulated during a counting period. Figure 5.5 illustrates the translation of the co-ordinates of a data point (x_i, y_i) to (x_{i+1}, y_{i+1}).

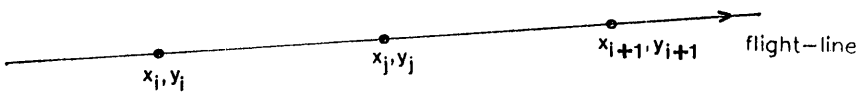

$$x_j = x_i + (x_{i+1} - x_i)/2$$

$$y_j = y_i + (y_{i+1} - y_i)/2$$

Figure 5.5 Translation of co-ordinate (x_i, y_i) to (x_{i+1}, y_{i+1}).

This step corrects for the procedural translation of data that would otherwise occur, as the data obtained over the interval from (x_i, y_i) to (x_{i+1}, y_{i+1}) are recorded at the latter co-ordinate, while actually more representative of a point midway along the counting interval.

Improvement of the statistical adequacy of the data

The third process was the improvement of the statistical adequacy of the data (Geometrics, 1984), and deals with the averaging of data within a moving window. Figure 5.6 shows the moving-window averaging operation.

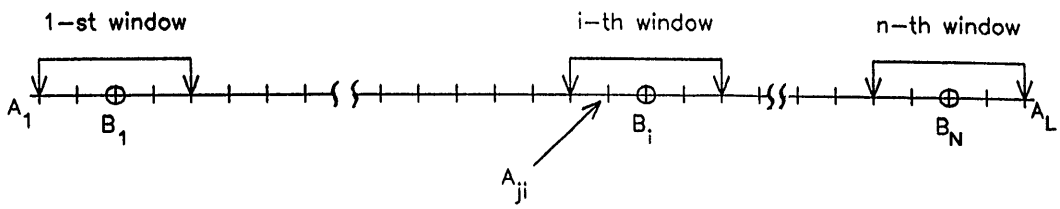

Figure 5.6 Moving-window averaging operation.

The value B_i replaces n consecutive data A_{ij} point within the window using the expression

$$B_i = \left(\frac{\sum_{j=1}^{n} A_{ji}^{\frac{1}{2}}}{n}\right)^2 \qquad 5-2.1$$

where

B_i = the average value obtained in the window of the ith data segment

A = the jth data point within the window of the ith data segment

i = 1,2,3,4,.....N

j = 1,2,3,4,.....n

N = number of data segments in a line of data

n = the width of the window

Expression 5-2.1 was chosen because the Poisson distribution governing counting statistics has a standard deviation equal to the square root of the number of counts in the counting interval.

For a line of data of length L, the number of data segments N can be expressed by the following relation

$$N = L - M - 1 \qquad 5-2.2$$

where $M = \frac{(n+1)}{2}$ is the centre of the window.

Background removal

The removal of background radiation was performed by subtracting the average value of the background radiation including cosmic ray background in each channel from data for the appropriate channels, using the relation

$$C_{T_b} = C_{T_r} - B_T \qquad 5-2.3(a)$$

$$C_{U_b} = C_{U_r} - B_U \qquad 5-2.3(b)$$

$$C_{K_b} = C_{K_r} - B_K \qquad 5-2.3(c)$$

$$C_{TC_b} = C_{TC_r} - B_{TC} \qquad 5-2.3(d)$$

where

- C_{T_b}, C_{U_b}, C_{K_b}, and C_{TC_b} are respectively background corrected count rate in the Th, U, K, and total- radiation (TC) channels;

- C_{T_r}, C_{U_r}, C_{K_r}, and C_{TC_r} are respectively raw count rate in the Th, U, K, and total-radiation (TC) channels;

- B_T, B_U, B_K, and B_{TC} are respectively the average background radiation count rate in the Th, U, K, and total-radiation channels.

Background radiation were measured by flying the gamma-ray spectrometer above body of waters at elevation of about 500 up to 1800 metres above mean sea level. Under this situation, radiation from source rocks below the water surface is effectively attenuated.

Spectral stripping

The spectral stripping for K and U channels was performed employing the following expression

$$C_{U_s} = C_{U_b} - S_{ut}C_{T_b} \qquad 5-2.4(a)$$

$$C_{K_s} = C_{K_b} - S_{ku}C_{u_s} - S_{kt}C_{T_b} \qquad 5-2.4(b)$$

where

C_{U_s} = stripped count rate in the U window;

S_{ut} = stripping coefficient in the U window due to Th interference;

C_{K_s} = stripped count rate in the K window;

S_{ku} = stripping coefficient in the K window due to U interference;

S_{kt} = stripping coefficient in the K window due to Th interference.

All stripping coefficients except for S_{ut} were considered constants. S_{ut} was treated as an altitude-dependent parameter which can be written in the following form (Grasty, 1975)

$$S_{ut} = S_{ut_0} + 0.00025h \qquad 5-2.5$$

where

S_{ut_0} = stripping coefficient in the U due to Th interference at the surface of the ground;

h = altitude in metres.

Altitude normalization

The altitude normalization was performed using the expression

$$C_{H_n} = C_{H_r} e^{\frac{H_n - H_r}{H_n}} \qquad 5-2.6$$

where

C_{H_n} = normalized count rate at the normalized altitude H_n;

C_{H_r} = normalized count rate obtained at the altitude H_r where measurements were conducted.

Filtering of the airborne radiometric data

The objective of the filtering of the airborne radiometric data was to determine the distribution of the true concentration of radioactive element present on the ground surface. A space-domain, wave-shaping, digital inverse-filter was used to deconvolute the corrected airborne radiometric data. The weights of the filter were derived utilizing the condition that the filter is optimum in an error-distribution sense (Mereu, 1978).

Theory

Given a point-source of a radioactive element on the ground surface, the spatial response of a γ-ray detector at a constant altitude h and distance x from the source (see Figure 5.7) may be written as follows

$$R(x) = \frac{NA\varepsilon}{4\pi r^2} e^{-\mu r}, \qquad 5-2.7$$

with

$$r^2 = h^2 + x^2,$$

and where

N = number of γ-ray photons emitted by the radioactive point-source per unit time;

A = effective area of the γ-ray detector;

ε = efficiency of the detector;

μ = attenuation coefficient for γ-ray of particular energy;

4π = geometric constant.

The function $R(x)$ does not represent the true concentration of the radioactive point-source. The true concentration of the source is given by the following expression

$$C(x) = \begin{cases} 1, & x = 0 \\ 0, & x \neq 0 \end{cases} \qquad 5-2.8$$

Figure 5.8 illustrates the true concentration of radioactive point-source situated on the ground surface.

The relation between $R(x)$ and $C(x)$ is given as follows

$$R(x) = C(x) * S(x) = \int_{-\infty}^{\infty} C(u)S(x-u)du \qquad 5-2.9$$

where $*$ denotes the process of convolution (Bracewell, 1978). $S(x)$ represents the combination of the spatial impulse-response of the medium and the temporal impulse-response of the γ-ray detecting system used in the survey.

In practical applications, $R(x)$ represents the recorded signal when a radiometric survey is being conducted. The recorded information is not a continuous function. It is a discrete sequence of numbers which may be represented as (Papoulis, 1980):

$$R[n] = R(nx) \qquad 5-2.10$$

where

$n =$ any integer number representing data taken in a discrete sequence (see Figure 5.9);

$x =$ sampling interval.

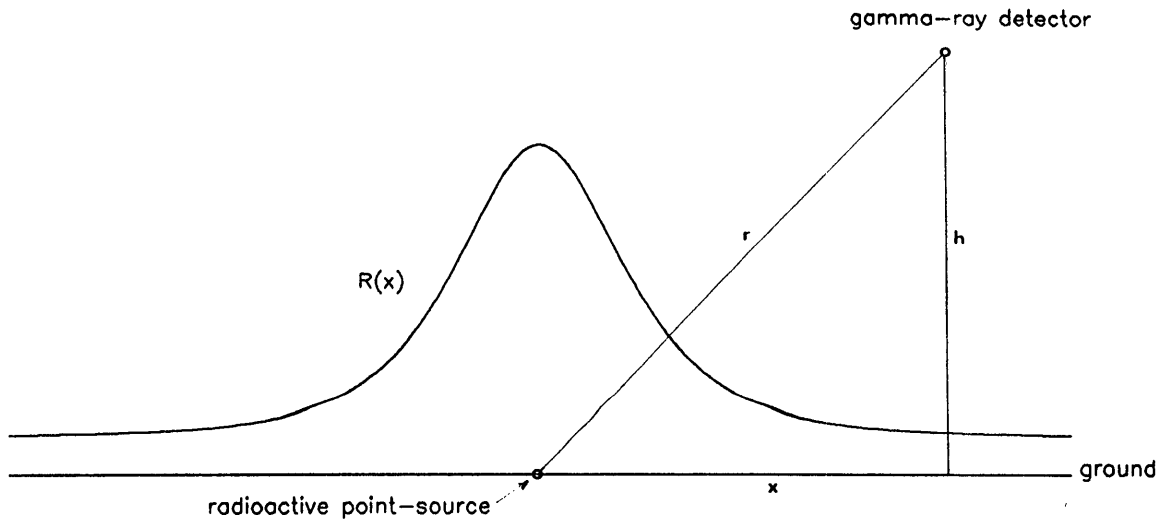

Figure 5.7 Spatial response of a gamma-ray detector due to a radioactive point source.

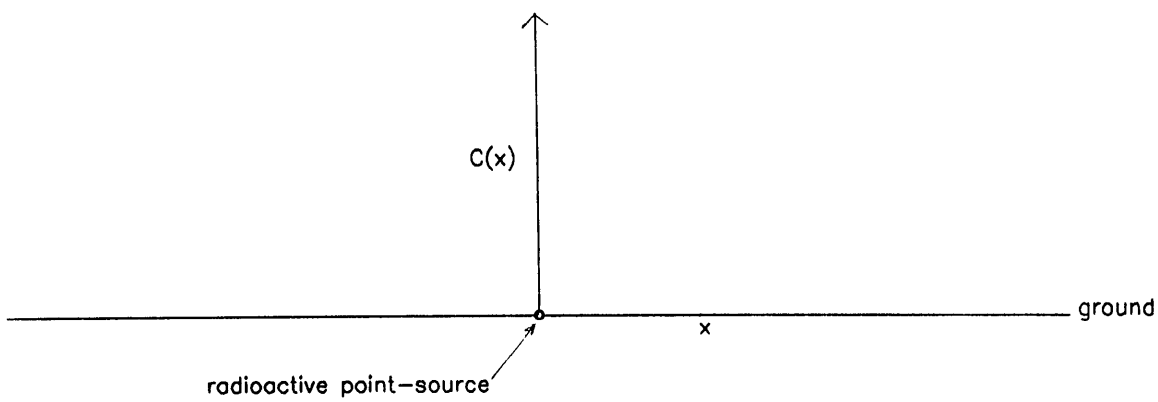

Figure 5.8 True concentration of a radioactive point-source, $C(x)$ has the value 1 at $x = 0$ and 0 elsewhere.

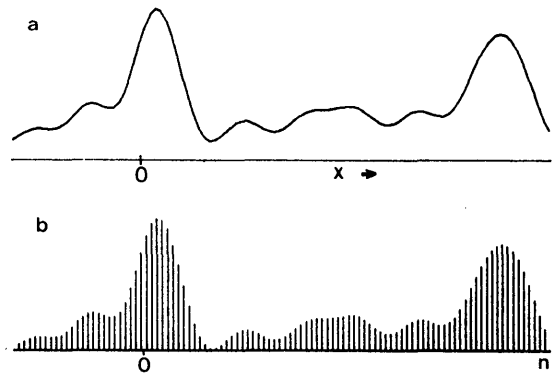

Figure 5.9 (a) continuous signal:

(b) discrete or sampled signal.

In discrete notation, equation 5-2.9 can be rewritten in the following form (Papoulis, 1980)

$$R[n] = C[n] * S[n] = \sum_{k=0}^{N} C[k] S[n-k] \qquad 5-2.11$$

The recorded information $R[n]$ is a representation of the true concentration $C[n]$ convoluted with the spatio-temporal impulse-response $S[n]$.

It is desired to recover the true concentration of the radioactive point-source $C[n]$ from the recorded data $R[n]$. To perform this recovery, an inverse filter $F[n]$ of the impulse-response $S[n]$ must be evaluated such that

$$R[n] * F[n] = C[n] \qquad 5-2.12$$

Equation 5-2.12 demonstrates that the convolution of the inverse filter $F[n]$ and the recorded information $R[n]$ gives the desired waveform which represents the distribution of true concentration of radioactive elements present on the ground surface.

Figure 5.10 illustrates the recovered waveform $A[n]$ from the recorded information $R[n]$ which has been convoluted with the inverse filter $F[n]$ if the desired waveform is $C[n]$. The recovered waveform $A[n]$ differs from the desired waveform in that $A[n]$ contains minor spikes on either side of the primary spike. The small spikes on the side lobes show the Gibb's phenomenon which is mainly caused by the finiteness in the length of a line of data (Hamming, 1977) and the discontinuity of the function $C[n]$ (Papoulis, 1980).

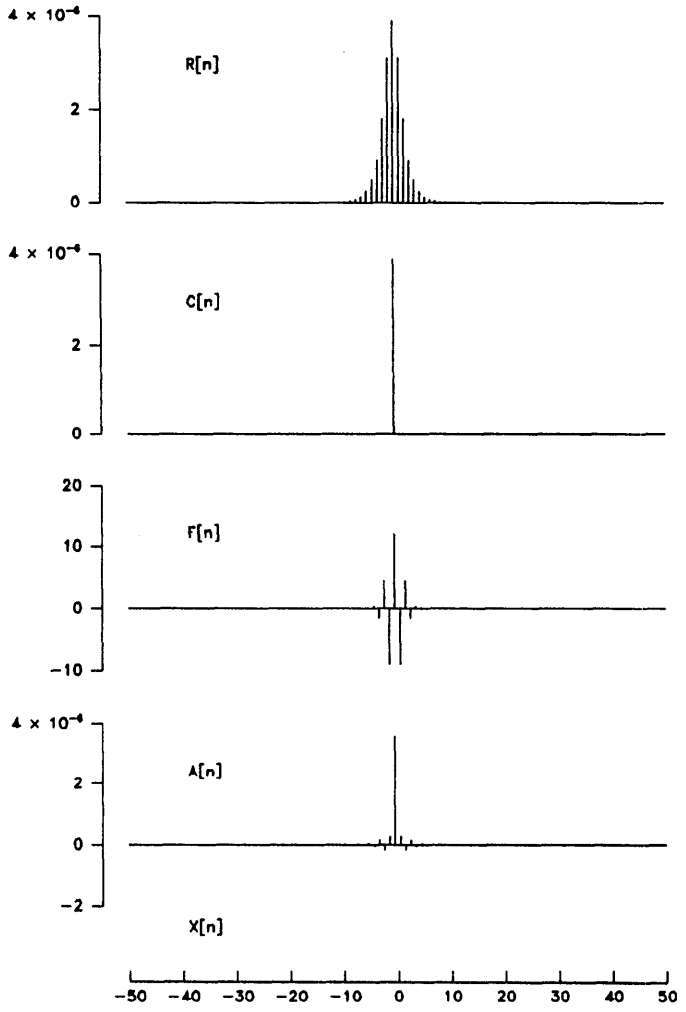

Figure 5.10

(a) the discrete spatial response of a gamma-ray detector due to a radioactive point-source $R[n]$;

(b) the desired waveform which represents the true concentration of the radioactive source on the ground $C[n]$;

(c) the weights of the space-domain wave-shaping inverse filter $F[n]$;

(d) the recovered waveform $A[n]$ which is often referred to as the actual output of the deconvolution process;

(e) distance along the sampling line $X[n]$.

Design of the space-domain digital inverse filter (After Mereu, 1976)

Let A be a symmetrical discrete series of spatial variables of the following form

$$A = [a, 1, a]$$
$$B = [-a, 1, -a]$$

then

$$A * B = [a, 1, a] * [-a, 1, -a]$$
$$= [-a^2, 0, 1 - 2a^2, 0, -a^2]$$

When the signs of alternate values of a symmetric discrete series are reversed, and the newly created series is convoluted with the original series, the resultant series will have its alternate values exactly equal to zero.

Zero values may also be inserted in the series when the multiplication between the z-transforms of A and B is performed.

$$\text{The } z\text{-transform of } A = [a, 1, a] \text{ is}$$
$$= az^{-1} + 1 + az$$

and

$$\text{the } z\text{-transform of } B = [-a, 1, -a] \text{ is}$$
$$= -az^{-1} + 1 - az$$

and the multiplication between the z-transforms of A and B is performed as follows

$$
\begin{array}{lll}
 & az^{-1} + 1 + az & \\
 & -\ az^{-1} + 1 - az & \times \\
\hline
-\ a^2z^2 - az^{-1} & - & a^2 \\
 & + az^{-1} + 1 & + az \\
 & - & a^2 - az - a^2z^2 \\
 & & + \\
\hline
-\ a^2z^2 + 0z^{-1} & & +(1 - 2a^2) + 0z - a^2z^2
\end{array}
$$

More zero numbers will be inserted into the output waveform when the operation is repeated.

$$
\begin{aligned}
&= \left[\ -a^2,\ 0,\ 1 - 2a^2,\ 0,\ -a^2\right] * \left[\ a^2,\ 0,\ 1 - 2a^2,\ 0,\ a^2\ \right] \\
&= \left[\ -a^4,\ 0,\ 0,\ 0,\ 1 - 4a^2 + 2a^4,\ 0,\ 0,\ 0,\ -a^4\ \right]
\end{aligned}
$$

If the operation is repeated N times, the number of zeros which are inserted will be $2^N - 1$.

To evaluate the weights of the filter $F[n]$ in equation 5-2.12, the following formula has been used

$$F[n] = F_0[n] * F_1[n] * F_2[n] * \ldots\ldots\ldots\ldots * F_N[n] * C[n] \qquad 5-2.13$$

where

$C[n] =$ the desired waveform;

$F[n] =$ the filter;

$F_0[n] =$ the sequentially-reversed R[n];

$F_1[n] = R[n] * F_0[n]$, with signs of alternate terms reversed;

$F_2[n] = R[n] * F_0[n] * F_1[n]$,with signs of alternate non-zero terms reversed;

$F_3[n] = R[n] * F_0[n] * F_1[n] * F_2[n]$, with signs of alternate non-zero terms reversed;

.

.

.

$F_N[n] = R[n] * F_0[n] * F_1[n] * F_2[n] * \ldots * F_{N-1}[n]$, with signs of alternate non-zero terms reversed;

$N =$ the number of sub-filters to be used in the evaluation of the filter $F[n]$.

The computer program FILTER evaluates the space-domain wave-shaping digital inverse filter $F[n]$. It is a modified version of the computer program which was published by Mereu (1978).

Deconvolution process of the airborne radiometric data

Three computer programs were used to perform inverse filtering of the airborne radiometric data. These were the RADXH, the SHAPER and the CONFIL computer programs. Figure 5.11 illustrates the filtering process of the airborne radiometric data.

The RADXH program computes the discrete theoretical spatial response of the γ-ray detector at the normalized altitude of the airborne survey. The airborne radiometric data were corrected and normalized to 122.0 metres mean terrain clearance. The FILTER computer program evaluates the weights of the inverse filter of the theoretical response of the gamma-ray detector given by the RADXH program. The CONFIL program performs the convolution process between the inverse filter and the airborne radiometric data. For practical purposes, the inverse filter has been truncated to 2.0 kilometres length (Green, 1985, pers. comm.).

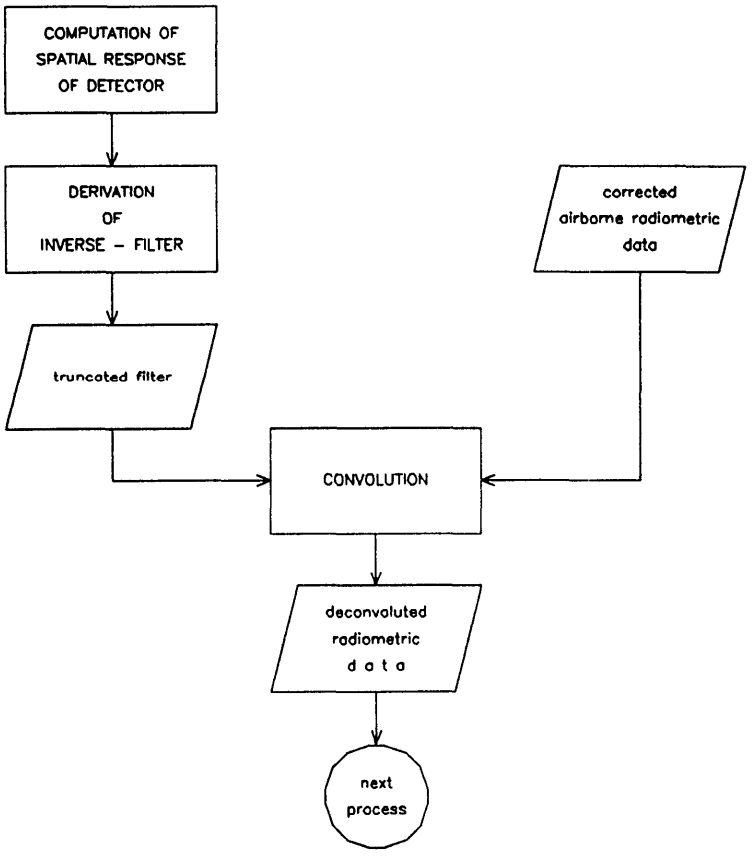

Figure 5.11 Inverse-filtering procedure of the airborne radiometric data.

Spatial-variation analysis of the airborne radiometric data

The objective of this analysis was to determine the spatial variation of the apparent concentration of radioactive elements present on the ground surface. The analysis also provided weighting coefficients which were used, subsequently, for generating the equally-spaced data. The regularly-gridded data were fed into the map-plotting routine to create colour maps which represent the apparent concentration of radioactive elements.

The computer programs VAR2DX (Balia, 1983) and VARMOD (Balia, 1983) were used to perform the analysis. Limitations on the usage of array-size and CPU-time on the DEC-20R computer system, under the current operating system, has prevented the analysis of the whole study area conducted at one time. The analysis was performed per flight-line in east and west directions, and in north-south directions for the tie-line data. The results from the analysis of every line of data were averaged and then used as the weighting factors for creating the gridded data using the kriging computer program, KRIG2D (Balia, 1983).

The transition-model variogram was used for analysing the data, because of its applicability to natural phenomena (Balia, 1983). This type of variogram has a "nugget effect", a "sill", and a "range of influence". The nugget effect is the discontinuity of the variogram at the origin. This discontinuity is caused by error in the measurement and micro-variabilities in the data (Journel and Huijbregts, 1978). The sill is the limit value where the variogram ceases to increase. The range of influence is the range or zone beyond which the influence of samples disappears. This range is indicated by the more or less stable values of the variogram.

Gridding the airborne radiometric data

The aim of this process was to generate a set of equally-spaced data. The computer program KRIG2D (Balia, 1983) was used to perform the interpolation. The program is an implementation of the kriging method which provides unbiased estimation on a set of regularly-spaced data. In the interpolation process, the kriging method takes into account the spatial variability of the data. The octant-search option of the program was utilized for ensuring a balanced distribution of samples, not only by lateral distance, but also in radial direction. The octant-search method selects the first N closest samples which fall within every sector of the octants. N is the number of samples within an octant sector.

Conversion of normalized count-rate to elemental concentration

The conversion factors for expressing the normalized count rate of the airborne radiometric parameters into elemental concentration were obtained using the 1022 Data Base System (Software House, 1980) and the Minitab Statistics Package (Pennsylvania Univ., 1981). The sorting and searching option of the 1022 Data Base System and the correlation analysis in the Minitab Statistics Package were used to evaluate the conversion factors. Figure 5.12 illustrates the procedure for obtaining the radiometric conversion factors.

Coincident co-ordinates, within a tolerated zone, between the corrected airborne data and the experimental ground radiometric data as described in Chapter 4 were sorted, such that the closest co-ordinates, with associated values, of the airborne radiometric data to the selected ground radiometric data can be isolated. Linear-regression analysis was then performed on the set of isolated data-pairs. The analysis provides correlation factors between the normalized count rate of the airborne radiometric data and the elemental concentrations measured in the experimental ground radiometric survey. Figure 5.13 illustrates the crossing-points between the experimental ground radiometric survey traverse and the airborne radiometric flight lines, showing circles of the tolerated zone of coincidence. Circles with the radius of 500.0 metres were used in the sorting procedure.

Results of this analysis for the Silent-Grove Road survey line appear in Chapter 6.

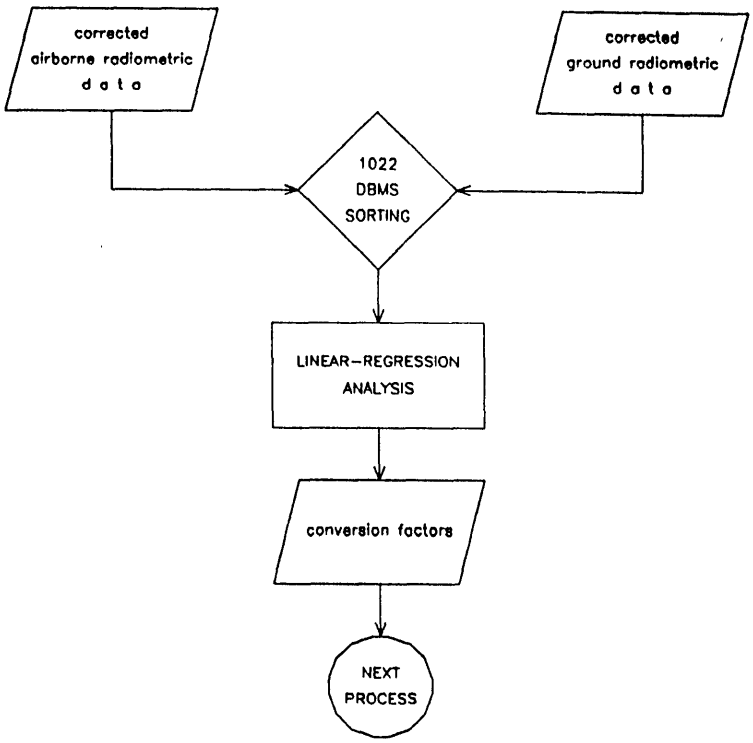

Figure 5.12 Sorting and correlation analysis of the airborne and experimental ground radiometric data.

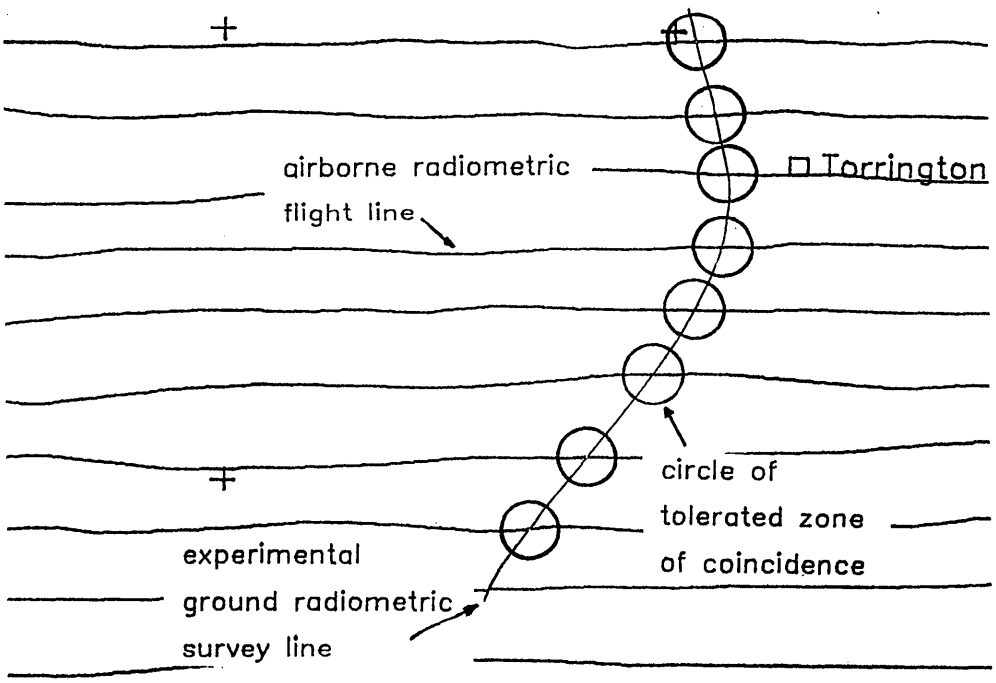

Figure 5.13 Crossing points between the airborne survey flight lines and the experimental ground survey traverse. (circles exagerated for clarity, not to scale.)

Plotting of the coloured maps of the airborne radiometric data

Program COLMAP was written, based on the ⟨PLOT79⟩ graphic software (Beebe, 1982) in order to produce the coloured maps presented in this thesis. The application program PV (Creedy, 1985) was used to plot the output from program COLMAP on a Hewlett-Packard HP-7475A six-pen plotter. The limited range of the HP's colour pens has restricted the drawing of the coloured maps to nine colours.

The classification of the mapped data into these nine intervals more or less follows equal-interval data-grouping (Howarth, 1983). The grouping was performed using the sorting capabilities of the 1022 Data Base System (Software House, 1980). Figure 5.14 shows a typical histogram of the nine-interval data-grouping used for mapping the airborne radiometric data.

Coloured maps of the airborne radiometric parameters K, eU, and eTh, and the ratio parameters eU/K, eU/eTh, and eTh/K are presented in the appendix volume of this thesis.

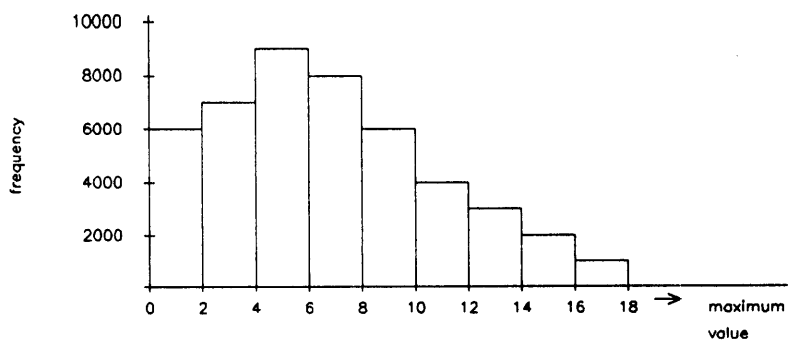

Figure 5.14 Nine-interval data-grouping of the airborne radiometric data.

5-3 Data processing of the experimental ground radiometric survey

The main objective of processing the experimental ground radiometric survey data was to provide corrections to the raw data and present the results in terms of radioelement concentration. These were percentage of K, μg/g of eU, μg/g of eTh, and the ratio concentration of eU/K, eU/eTh, and eTh/K were also presented.

Since the method of the experimental ground radiometric survey was a simulation of the integration of the airborne survey the processing method applied was in principle similar to that used for the airborne survey data.

Figure 5.15 is a flow diagram describing the processing of the experimental ground radiometric data. The computer program GXPRAD is the implementation of that processing sequence.

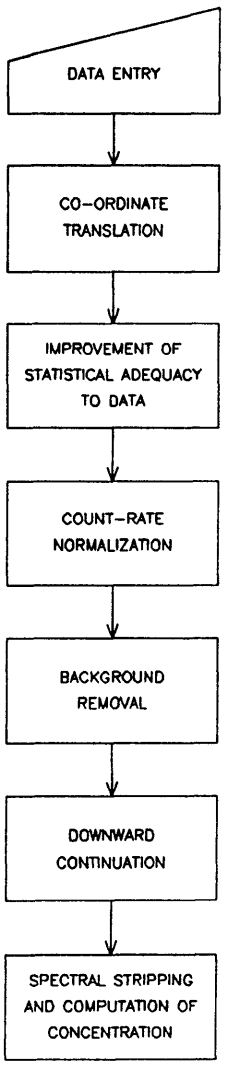

Figure 5.15 Flow diagram of data processing of the experimental ground radiometric survey.

The function of each section of the flow diagram is expanded in the following list.

Data entry

The intensities of radiation of each element recorded by the GAD-6/GSP-4 gamma-ray spectrometer were transferred manually into a field note-book. Apart from the radiometric parameters, the environment variables such as soil-wetness, crop-density, ratio between outcrop of rock units to soil-cover, distance of traverse, were also taken into consideration. These field-parameters were entered manually into the DEC-20R computer system.

Translation of co-ordinates

This step performs translation of the co-ordinate of a sampling point to a position which lies between its previous position and the position of the next sampling point. The position which results from the translation is associated with a value accumulated during an integration period over a certain coverage of traverse distance.

Improvement to statistical adequacy of data

This processing step performs a moving-average operation within a certain width of data-window over a line of data. The averaging algorithm used was similar to that applied to the airborne radiometric data.

Count-rate normalization

This procedure converts the raw count-rate into count-rate per second, by dividing the raw count-rate by the selected integration time.

Background removal

The background radiation was removed by subtracting the normalized background readings obtained on a two-hectare dam in Torrington from the normalized radiation count rate for the appropriate channels.

Downward continuation to ground surface

This processing step performs transformation of radiation count rate at 800.0 millimetres above the ground to the surface of the ground. The purpose of the transformation was to comply with the so-called 2π-geometry, that is, the situation in which the gamma-ray detector is sitting on top of the ground surface. This step was undertaken because the calculation of the concentration of radioelements, for the GAD-6/GSP-4 spectrometer, is to be performed for 2π-geometry. The transformation of the radiation count rate from 800.0 millimetres to 2π-geometry was carried out using the attenuation coefficients obtained from the Moonbi-Hills radiometric experiments. Equation 5-3.1 illustrates the downward continuation from 800.0 millimetres to 2π-geometry.

$$N_{2\pi} = \frac{N_{800}}{e^{-\mu h}} \qquad 5-3.1$$

where

$N_{2\pi}$ = the normalized count-rate at 2π-geometry;

N_{800} = the normalized count-rate at height 800.0 millimetres;

μ = attenuation factor for γ-ray photons of a particular energy;

h = height above ground surface.

Spectral stripping and calculation of concentration of radioelements

The procedure of spectral stripping and the evaluation of concentration of each radioelement was performed in accordance with the following equations (Scintrex, 1978)

$$eTh = \frac{1}{K_1} C(Th) \qquad 5-3.2(a)$$

$$eU = \frac{1}{K_2} \left[C(U) - \alpha C(Th) \right] \qquad 5-3.2(b)$$

$$K = \frac{1}{K_3} \left[C(K) - \gamma \left[C(U) - C(Th) \right] - \beta C(Th) \right] \qquad 5-3.2(c)$$

where

eTh = equivalent concentration of thorium (μg/g);

eU = equivalent concentration of uranium (μg/g);

K = concentration of potassium (%);

C(Th) = background corrected count rate in Th channel (counts per second);

C(U) = background corrected count rate in U channel (counts per second);

C(K) = background corrected count rate in K channel (counts per second);

K_1 = intensity calibration-constant for thorium (count rate per unit-concentration);

K_2 = intensity calibration-constant for uranium (count rate per unit-concentration);

K_3 = intensity calibration-constant for potassium (count rate per unit-concentration);

α = stripping coefficent for the U window as a result of interference from Th;

β = stripping coefficient for the K window as a result of interference from Th;

γ = stripping coefficient for the K window as a result of interference from U.

The corrected experimental ground radiometric survey data were used to provide correlation factors to a set of selected data from the airborne radiometric survey. This allowed the conversion of the normalized count-rate of the airborne radiometric data into elemental concentrations.

The results of the experimental ground radiometric survey are presented in the form of profiles of radiometric parameters, namely, total-radiation counts, percentage concentration of potassium (% K), equivalent concentration of uranium (μg/g eU), equivalent concentration of thorium (μg/g eTh). The ratio parameters such as eU/K, eU/eTh, and eTh/K are also presented in the same format. These profiles of radiometric parameters appear in Chapter 6 of this thesis.

5-4 Data processing of laboratory gamma-ray spectrometric analysis of rocks

The aim of processing the laboratory gamma-ray spectrometry data was to evaluate the concentration of radioelements K, U, and Th present in the rock samples. The concentrations were standardized using the international standard rock-samples GSP-1, AGV-1, BCR-1, and G-2. The background counts were obtained from the Dunite sample which contains negligible thorium, uranium, and potassium concentrations.

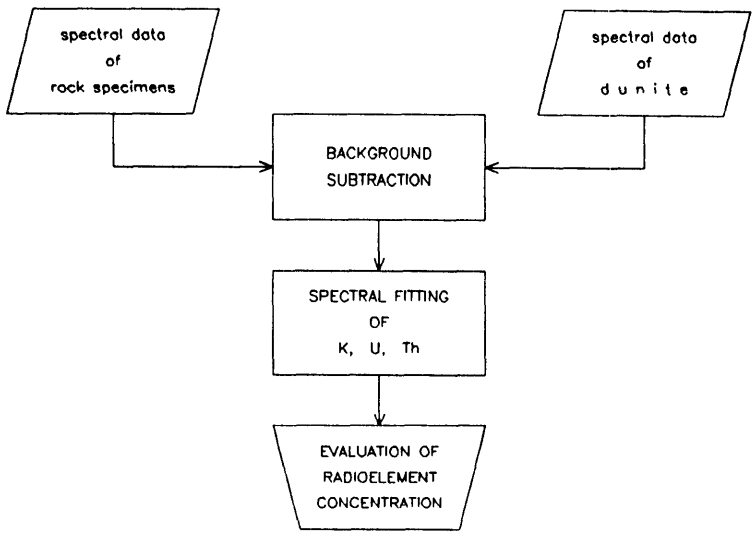

Figure 5.16 Flow diagram of the spectral curve fitting in the gamma-ray spectrometric analysis.

Least-square polynomial curve-fitting was employed to determine the analytical spectral peaks of individual radioelements. This routine provided an estimation of errors within the energy bands of K, U, and Th, giving the basic statistical measures of the observed energy spectrum. This subsequently allowed easy calculation of radioelement concentrations to be performed.

The computer program SPEFIT is the implementation of the data processing described above. The flow chart of the program is shown in Figure 5.16. The data transfer from the spectrometer, ORTEC-6240, was performed using the communication program MPREAD (Porter, 1983). The MPREAD program also performs formatting of the spectral data, allowing easy handling for subsequent analysis.

The removal of the background counts was performed by subtracting the Dunite spectral data from the spectral data of rock sample under investigation.

Polynomial curve-fitting for K, U, and Th energy bands was carried out by calling the NAG library subroutine E02ACF (NAG, 1981). This subroutine evaluates a minimax polynomial fit to a set of data points.

Given a set of data points $(x_i, y_i), i = 1, 2, 3, 4, \ldots\ldots\ldots\ldots, N$ in the arrays X and Y, both of dimension N, the routine uses the exchange algorithm to evaluate an M-th order polynomial of the following form

$$P(x) = a_1 + a_2 x + a_3 x^2 + a_4 x^3 + \ldots\ldots\ldots\ldots + a_{M+1} x^M \qquad 5-4.1$$

such that

$$\mathrm{Max}_i |P(x_1) - Y_i| \text{ is minimum}$$

Results of the laboratory γ-ray spectrometry analysis are presented in Chapter 6 of this thesis.

Chapter 6

RESULTS

6-1 Introduction

This chapter is concerned mainly with a description of the results of the study. These are presented in the appendix volume of this thesis.

Results from the airborne radiometric survey are presented in the form of coloured maps of total radiation, potassium concentration (K), equivalent uranium concentration (eU), and equivalent thorium concentration (eTh). Coloured maps of ratio parameters, namely, eU/K , eU/eTh , and eTh/K are also furnished.

Results from the experimental ground radiometric survey are presented in the form of profiles of parameters similar to those presented from the airborne survey. These results also provide correlation coefficients of the experimental ground radiometric data to the airborne radiometric data. The correlation coefficients obtained from the experiment were used to convert the normalized count rate of the airborne radiometric data into concentrations of radioactive elements potassium (K), equivalent uranium (eU), and equivalent thorium (eTh).

Results from the laboratory γ-ray analysis are presented in the form of a tabulation of concentrations of radioactive elements of rock samples collected from the field. Figures illustrating the fitting of curves to the spectral data of the rock samples are also included.

For the purpose of referencing grid localities of some areas, the topographic map of the study area is supplied (Figure A6.1).

Figure A6.2 is a geological map overlay which is intended for comparing the colour images on the radiometric maps and the distribution of rock types in the study area.

Figure A6.3 is an overlay depicting the locations of known ore deposits in the Mole Granite and surrounds. This transparency may be used for examining the coincidence between the known areas of ore mineralization and colour patterns on the corrected-and-deconvoluted maps of radiometric parameters. This may also be used for locating other areas which have potential for ore mineralization.

6-2 Results from the airborne radiometric survey

The flight paths of the airborne radiometric survey

The study area was covered by ninety-two survey flight lines and two survey tie-lines. Figure A6.4 shows the flight paths of the airborne radiometric survey. The paths were drawn by connecting consecutive co-ordinate points of data with a straight line. The average distance between two consecutive data points is approximately 50 metres. Arrow heads on the flight lines indicate the aircraft heading when the survey was conducted.

The airborne radiometric maps

The airborne radiometric maps which are described in this section are grouped into two classes. These are:

(a) maps of corrected data, and

(b) maps of corrected-and-deconvoluted data.

The correction and deconvolution of the data are described in Chapter 5 of this thesis.

Both types of maps have nine colour intervals. The colour grades which were used for drawing the maps have been set in the following order:

COLOUR		RANGE
1.	blue	lowest
2.	turquoise	.
3.	green	.
4.	lime green	.
5.	brown	.
6.	gold	.
7.	burnt orange	.
8.	red	.
9.	purple	highest

A coarser classification scheme has been defined by grouping the nine colour intervals into three levels. These are :

1 Low: blue, turquoise, and green as the first group which represents the low range of values on the map;

2 Medium: lime green, brown, and gold as the second group of colours for displaying the medium range of values on the map;

3 High: burnt orange, red, and purple as the third group of colours which can be assigned the high range of values on the map.

(a) Maps of corrected data of the airborne radiometric survey

The following maps of corrected data of the airborne radiometric survey represent the spatial response of the γ-ray detecting system used. This response, in general, characterizes the distribution of rock types in the area under investigation:

(1) Total radiation count (counts per second, cps) - Figure A6.5.

(2) Potassium concentration (%) - Figure A6.6.

(3) Equivalent uranium concentration (μg/g eU) - Figure A6.7.

(4) Equivalent thorium concentration (μg/g eU) - Figure A6.8.

(5) Concentration ratio of eU/K (dimensionless units) - Figure A6.9.

(6) Concentration ratio of eU/eTh (dimensionless units) - Figure A6.10.

(7) Concentration ratio of eTh/K (dimensionless units) - Figure A6.11.

Radiometric signature of the Mole Granite

The Mole Granite is located in the central portion of the study area. Examination of the above figures has yielded the observation that the granite is delineated by:

- total radiation intensities of 2 500 - 6 280 cps (Figure A6.5)
- potassium concentrations of 2.5 - 5.35 % (Figure A6.6)
- equivalent uranium concentrations of 2.0 - 16.0 μg/g eU (Figure A6.7)
- equivalent thorium concentrations of 10.0 - 53.20 μg/g eTh (Figure A6.8)
- eU/K concentration ratios of 1.5 - 4.0 (Figure A6.9)
- eU/eTh concentration ratios of 0.075 - 0.29 (Figure A6.10)
- eTh/K concentration ratios of 6.0 - 15.95 (Figure A6.11)

Patterns with a lower range of values of radiometric parameters also exist within the Mole Granite. This variation is caused primarily by :

(*1*) variation in rock types; and

(*2*) variation in soil or alluvial cover, and degree of weathering.

(1) Variation in rock types

A change in rock types generally results in a considerable amount of variation in the values of the radiometric parameters. Two areas on the Mole Granite exhibit this effect.

(i) The roof pendant

The roof pendant is situated 5 kilometres to the north west of the township of Torrington. This area is defined by patterns on Figures A6.5 - A6.8 of:

- total radiation (1 000 - 2 500 cps)
- potassium concentration (0.5 - 1.5 %)

- equivalent uranium concentration (0.0 - 4.0 μg/g eU)

- equivalent thorium concentration (0.0 - 15.0 μg/g eTh)

All of these depleted values of radiometric parameters signify the Permo-Carboniferous sedimentary rocks which formed the roof pendant.

The location of the roof pendant is less clearly defined in the remaining three Figures (A6.9 - A6.11):

- eU/K concentration ratio. The eastern and northern margins of the roof pendant are characterized by medium range ratio values of 2.0 - 3.0 . The central portion and the western margin of the pendant are indicated by lower ratio values of 0.5 - 2.0 .

- eU/eTh concentration ratio. The central and western parts of the roof pendant show patterns with ratio values ranging from 0.025 to 0.100. On the eastern part of the pendant, patterns with ratio values between 0.100 - 0.175 clearly dominate the area.

- eTh/K concentration ratio. The central part of the roof pendant is characterized by ratio values of 4.50 - 7.50 . Patterns with high ratio values ranging from 9.00 to 15.95 prominently appear at the outer margin of the pendant.

(ii) The I-type granite

This unit outcrops on an area situated 2 kilometres to the east of Torrington. This area is defined by patterns on Figures A6.5 - A6.8 of:

- total radiation (1 500 - 2 000 cps)

- potassium concentration (1.5 - 2.0 %)

- equivalent uranium concentration (0.0 - 2.0 μg/g eU)

- equivalent thorium concentration (5.0 - 10.0 μg/g eTh)

The above indicate that an I-type granite has a weaker radiometric response compared with an A-type granite. A detailed analysis of the I-type granite from this area is shown in Tables 6-4.2 and 6-4.3 of this thesis.

The location of the I-type granite is clearly defined in the remaining Figures (A6.9 - A6.11):

- eU/K concentration ratio (0.50 - 2.0)
- eU/eTh concentration ratio (0.025 - 0.100)
- eTh/K concentration ratio (1.5 - 6.0).

Results from major element analysis in Table 6-4.2. show higher values compared to the maps of corrected data of the airborne radiometric survey in this particular area. Maps which were produced from corrected-and-deconvoluted data show values closer to the results from the elemental analysis (see Figure A6.12 through A6.17).

(2) variation in soil or alluvial cover and degree of weathering

Variation in the thickness and extent of soil or alluvial materials which cover the surface of the Mole Granite can produce a masking effect to the γ-rays which are emitted from the granite.

This effect can be seen on an area situated 10 kilometres to the north-north-east of Torrington, in which a wide valley of alluvial sediments has caused attenuation of the total radiation, reducing the intensities down to 1 000 - 2 500 cps on the map of total radiation count (Figure A6.5). (See also the topographic map in Figure A6.1 for locating this area). In particular this area has been characterized by the following ranges for the various radiometric parameters:

- potassium concentration, 1.0 - 2.5 % (Figure A6.6)
- equivalent uranium concentration, 0.0 - 2.0 μg/g eU (Figure A6.7)
- equivalent thorium concentration, 5.0 - 20.0 μg/g eTh (Figure A6.8)
- eU/K concentration ratio, 0.50 - 1.0 (Figure A6.9)
- eU/eTh concentration ratio, <0.075 (Figure A6.10)
- eTh/K concentration ratio, 7.5 - 13.5 (Figure A6.11). This pattern does not clearly define the area. Only a trace of high values (10.5 - 12.0) indicates where an extensive alluvial material masked the Mole Granite.

Radiometric signature of the sedimentary rocks surrounding the Mole Granite.

On the total radiation map (Figure A6.5), radiation intensities of 1 000 - 1 500 cps exhibit good coincidence with the Permo-Carboniferous Sedimentary rocks which outcrop extensively on the northern half and south west part of the study area.

Potassium concentrations, ranging from 1.5 - 2.0 %, show good correlation with the sedimentary terrain (Figure A6.6). Smaller patterns of high concentrations (2.0 - 3.5 %) dominate the north west corner of the study area. This area is also composed of sedimentary rocks of similar age. Patterns with a similar range of concentrations also exist on an area situated 5 - 10 kilometres to the north and north west of Emmaville.

Concentrations of 0.0 - 2.0 μg/g eU (Figure A6.7), in general, exhibit very good correlation with the Permo-Carboniferous sedimentary rocks in the study area. Minor patterns with higher concentrations (2.0 - 4.0 μg/g eU) are scattered unevenly on the northern part of the area which is also composed of similar types of rocks.

On the map of equivalent thorium concentration (Figure A6.8), the dominant feature with concentration of 5.0 - 10.0 μg/g eTh coincides with the distribution of the sedimentary rocks mentioned.

eU/K concentration ratios within the range of 0.0 - 1.0, generally display a very good coincidence with the Permo-Carboniferous sedimentary terrain (Figure A6.9). On the south west half of the Mole Granite, these sedimentary facies show reasonable correlation with patterns representing similar ranges of ratio values.

Patterns with ratio values within the range of 0.0 - 0.05 on the eU/eTh concentration ratio map (Figure A6.10), coincide with the distribution of the outcrops of the sedimentary rocks to the northern and south western part of the Mole Granite. Patterns with higher values of concentration ratio, especially on the area near the south west contact with the Mole Granite and on an area to the north and north west of Emmaville, also coincide with the sedimentary rocks mentioned.

On the map of eTh/K concentration ratios (Figure A6.11), ratio values within the range of 0.0 - 3.0 delineate the exposed Permo-Carboniferous sedimentary units in the study area.

Radiometric signature of the volcanic rocks

The following volcanic units were defined on the map of total radiation count (Figure A6.5):

- Permian Volcanics (outcropping), 1 000 - 3 000 cps.
- Emmaville Volcanics, 1 000 - 3 000 cps.
- Tent Hill Porphyrite, 2 000 - 2 500 cps.
- Dundee Rhyodacite, 1 500 - 2 000 cps in the areas closer to the Tent Hill Porphyrite and a lower range of intensities of 1 000 - 1 500 cps towards the south east corner of the study area.
- Gibraltar Ignimbrite, 2 000 - 3 000 cps. (6 kilometres to the north-north-east of Silent Grove).
- Minor outcrops of volcanic rocks on the east and north east corner of the area, 2 000 - 3 000 cps.

On the map of potassium concentration (Figure A6.6), the volcanic units in the study area are chiefly displayed by patterns with concentration range of 1.5 - 3.0 %. Patterns with a higher range of concentration (3.0 - 5.35 %) also appear in some areas. The following volcanic units were defined:

- Emmaville Volcanics, 2.0 - 4.0 % Patterns with a lower concentration (0.0 - 1.5 %) also appear towards the boundary of the Tertiary Basalt.
- Tent Hill Porphyrite, 2.0 - 3.0 %
- Dundee Rhyodacite, 2.0 - 3.0 % on the areas near the Tent Hill Porphyrite. A pattern with a lower range of potassium concentration (1.0 - 2.0 %) also coincides with the Tent Hill Porhyrite.
- volcanic facies (outcropping) on the north east corner of the study area, 3.0 - 5.35 %
- Gibraltar Ignimbrite, 2.5 - 5.35 %

On the equivalent uranium concentration map (Figure A6.7), the volcanic rocks in the study area do not exhibit a distinct response if compared with the Permo-Carboniferous sediments. However, there are some patch-like patterns which delineate the volcanic units which have a slightly high eU content.

- Emmaville Volcanics, 2.0 - 6.0 μg/g eU in the southern portion, whereas, the north portion, which is situated near the Tertiary Basalt, shows a similar response to the sedimentary rocks.

- Tent Hill Porphyrite, sharply defined by concentrations of 2.0 - 4.0 μg/g eU. On the area close to the Mole Granite, this unit shows a similar signature to the sedimentary facies.

- Dundee Rhyodacite, in general, exhibits a similar response to the Permo-Carboniferous sedimentary rocks.

- minor volcanic rocks on the north east corner of the study area are indicated by concentrations of 2.0 - 4.0 μg/g eU.

- Gibraltar Ignimbrite, 2.0 - 4.0 μg/g eU.

On the map of eU/K concentration ratio (Figure A6.9), all of the volcanic units in the study area exhibit a similar signature to the Permo-Carboniferous sedimentary rocks except the Emmaville Volcanics which show a low to medium range of eU/K concentration ratio (0.50-1.5).

On the eU/eTh concentration ratio map (Figure A6.10), all of the volcanic rocks in the study area show a slightly better response than the sedimentary rocks. However, this response is only characterized by patterns with ratio values of not more than 0.10.

On the eTh/K concentration ratio map (Figure A6.11), the volcanic units are signified by ratio values of 1.50 - 6.0. A higher range of ratio values are found on an area to the south west of Emmaville with ratio values of 9.0 - 15.95. The Emmaville volcanics are, in general, within a pattern which has eTh/K ratio values of 1.5 - 6.0. These ratio values steeply increase as the volcanic rocks interface with the Tertiary Basalt. This interface is characterized by ratio values of 6.0 - 13.5 and higher.

Radiometric signature of the other types of granitic rocks

Apart from the Mole Granite, other granites which outcrop on the north east and east perimeter of the study area include the Undifferentiated Granite, the Clive Adamellite, the Pyes Creek Leucoadamellite, and the Bolivia Range Leucoadamellite. The Undifferentiated Granite also appears on the south west corner of the area.

The granites were characterized by the following radiation intensities and ratios on the respective maps:

- total radiation 2 000 - 3 500 cps (Figure A6.5),

- potassium concentration, 2.0 - 3.0 % (north east, east, and south west corner of the study area) (Figure A6.6).

- equivalent uranium concentration (Figure A6.7). This group of rocks does not show a distinct response if compared with the sedimentary and volcanic rocks in the area. This response is signified by patterns with concentration 2.0 - 4.0 μg/g eU situated on the north east and east part of the study area, and patterns with concentration of 2.0 - 6.0 μg/g eU on the south west corner of the area.

- equivalent thorium concentration, 10.0 - 30.0 μg/g eTh, situated on the north east, east, and south west part of the study area (Figure A6.8), demonstrate a strong coincidence with the areas on which these granitic units outcrop.

These values are typical of I-type granite of New England area which are lower particularly in eU and eTh.

- eU/K concentration ratio (Figure A6.9) does not clearly define any of the granitic units. However, small patterns with ratio values of 0.5 - 1.5 on the north east, east, and south west part of the study area, exhibit traces of outcrops of this group of granitic facies.

- eU/eTh concentration ratio (Figure A6.10), the I-type granites show similar ratios as for the surrounding sedimentary and volcanic rocks which have been characterized by patterns with ratio values not more than 0.10.

- eTh/K concentration ratios, 3.0 - 6.0 (Figure A6.11), situated on the north east, east, and south west corner of the study area, correlate well with exposed bodies of these granitic rocks. Higher ratio values of eTh/K (4.5 - 12.0) exist on the area where the Bolivia Range Leucoadamellite outcrops.

Radiometric signature of the Tertiary Basalt

The Teriary Basalt appears on the south west half of the study area. This unit also outcrops on the south east corner, extending from west of Deepwater to the area to the east of Stannum.

This unit is characterized by:

- total radiation, 500 - 1 500 cps (Figure A6.5)
- potassium concentration, 0.0 - 1.0 % (weak correlation) (Figure A6.6)
- equivalent uranium concentration, 0.0 - 2.0 μg/g eU (Figure A6.7). The basalt does not exhibit a distinct response compared with the surrounding sedimentary rocks.
- equivalent thorium concentration, 0.0 - 5.0 μg/g eTh (Figure A6.8).
- eU/K concentration ratio (Figure A6.9), shows poor correlation with areas of exposed basalt. However, the outcropped basalt generally produces low ratio values of this parameter.
- eU/eTh concentration ratio (Figure A6.10), the basalts are poorly defined by this parameter.
- eTh/K concentration ratio (Figure A6.11). Ratio values between 0.0 to 3.0 situated on the south west half of the study area coincide with portions of the exposed basalts. High ratio values (9.0 - 15.95) appear to have resulted from very low potassium concentrations and moderately high concentrations of equivalent thorium. On the south east half of the the study area, the basalt is not clearly defined by this parameter. However, patterns with medium to high ratio values situated 5 kilometres to the north west and 10 kilometres to the north-north-west of Deepwater show traces of the exposed basalt.

Radiometric signature of the known areas of ore mineralization

In areas where ore mineralization has occurred, there is a general, but not universal, indication of an abundance of certain types of radioelements. In some cases, ratio values of radioelements emphasize areas of interest. The following list describes the radiometric response of these areas.

- total radiation (Figure A6.5). Radiation intensities within the range 2 500 - 3 000 cps, situated 1 kilometre to the east of the township Emmaville, show good correlation with an open cut (chiefly cassiterite) mine (the Great Britain Stockworks). Some of the known areas of ore mineralization in the Mole Granite, generally, show a fairly good correlation with patterns which have a high range of radiation intensities (3 000 - 6 280 cps). However, in areas surrounding the Mole Granite, this parameter does not clearly define the areas of interest. These high radiometric values relate strongly to the stripping of the soil cover as a result of the open pit mining operation. There is also a possibility of enchancement due to hydrothermal alteration during mineralization.

- potassium concentration (Figure A6.6). The Great Britain Stockworks are characterized by low to medium potassium concentrations (2.5 - 3.5 %). On the Mole Granite, some areas with tin mineralization associated with pegmatites strongly coincide with high potassium concentrations, e.g. Garths lode and Stormers lode. Little or no correlation exists for areas with ore mineralization of different styles.

- equivalent uranium concentration (Figure A6.7). A small area with concentrations ranging from 4.0 - 6.0 μg/g eU, situated 1 kilometre to the east of Emmaville, correlates well with the location of the Great Britain Stockworks. Some areas on the Mole Granite, that have known ore mineralization associated with pegmatites, show good correlation concentrations ranging from 10.0 - 12.0 ug/g eU, e.g. Garths and Stormers lodes.

- equivalent thorium concentration (Figure A6.8). A small pattern with concentrations between 15.0 to 20.0 μg/g eTh, situated 1 kilometre to the east of Emmaville, coincides with the location of the Great Britain Stockworks. On the Mole Granite, patterns representing medium to high equivalent thorium concentrations (25.0 - 53.20 μg/g eTh), correlate well with areas of known ore mineralization. Outside the Mole Granite, this parameter generally shows little correlation with the known areas of ore mineralization.

- eU/K concentration ratio (Figure A6.9). The distinct pattern which delineates the Great Britain Stockworks is not apparent on this map. Some of the documented locations of ore mineralization on the southern half of the Mole Granite coincide with medium to high values of eU/K concentration ratio (2.0 - 4.0). The McKinnons and McCowens mica lode, for example, shows a high range of ratio values (3.0 - 4.0). Areas with known bismuth and wolframite mineralization appear to have a low range of eU/K concentration ratio (0.5 - 1.0). e.g., the Fielder Hill, Elliot and Hores lode, Trewhellas lode, and Saul and Saunders prospect. On areas surrounding the Mole granite, this radiometric parameter, generally, shows little indication of ore mineralization of those areas. However, the locations of deep lead cassiterite mines were found to have a high range of values of eU/K concentration ratio (3.0 - 3.5). These are the Spring Lead cassiterite mine and an area which is situated 5 kilometres to the north west of Deepwater. Several locations with

known alumina prospects situated within 10 to 15 kilometres to the west of Emmaville coincide well with medium to high values of eU/K concentration ratio (2.0 - 3.5). Patterns with ratio values between 1.5 to 3.0, situated immediately and approximately 5 kilometres to the south west of Emmaville, possibly indicate abandoned mining areas.

- eU/eTh concentration ratio (Figure A6.10). Several alumina prospects situated 16.5 kilometres to the west of Emmaville correlate well with high values of eU/eTh concentration ratio. The high eU/eTh ratio in this area may be due to the presence of clay. These clays may have been produced by hydrothermal alteration or deep weathering. The Spring lead prospect is also sharply defined by high eU/eTh concentration ratios. However, other prospects with a similar style of mineralization, which produced similar types of ore minerals, are not so readily indicated. This parameter was therefore considered unsuitable for assessing this type of ore mineralization.

- eTh/K concentration ratio (Figure A6.11). Medium to high values of this parameter (6.0 - 13.5 and higher) indicate some areas of mineralization situated in the Mole Granite. In areas outside the Mole Granite, ratio values of 10.5 - 13.5 and higher coincide with a deep-lead cassiterite mine situated 5 kilometres to the north west of Deepwater. However, some other locations with a similar style of ore deposit, e.g. Spring lead mine and Surprise mine (see Figure A6.3) do not show a similar indication.

(b) Maps of corrected-and-deconvoluted data of the airborne radiometric survey

The idea of the deconvolution was to separate the intrinsic impulse waveform from the spatial impulse response waveform which is analogous with the recorded data. All maps which have been created using the deconvoluted data tend to enhance high localized anomalies of radioelement concentration. At the same time the broad patterns related to the distribution of rock types are to some degree, supressed.

A high local anomaly, in general, signifies an area with a high potential of ore mineralization which is associated with a significant abundance of the radioelement parameters for potassium (K), equivalent uranium (eU), and equivalent thorium (eTh).

The following maps represent the corrected-and-deconvoluted data:

- Potassium concentration (%) - Figure A6.12.
- Equivalent uranium concentration (μg/g eU) - Figure A6.13.
- Equivalent thorium concentration (μg/g eU) - Figure A6.14.
- Concentration ratio of eU/K (dimensionless units) - Figure A6.15.
- Concentration ratio of eU/eTh (dimensionless units) - Figure A6.16.
- Concentration ratio of eTh/K (dimensionless units) - Figure A6.17.

Coincidence between radiometric parameters with the known areas of ore mineralization

(1) Areas of ore mineralization in the Mole Granite

On the potassium map (Figure A6.12), most of the known areas of ore mineralization coincide well with potassium concentrations within the range of 2.0 - 4.0 %. This indicates that the ore mineralization in these areas is related closely to the occurrence of potassium-rich compounds, e.g., ore mineralization associated with pegmatites. Lower potassium concentrations (0.5 - 2.0 %) also display a fairly good correlation with the areas of interest. This would indicate that a different style of ore mineralization has occurred in some areas, e.g., ore mineralization associated with aplitic granite dykes or aggregation of irregular minor veins.

Stronger correlation can be seen on the equivalent uranium map (Figure A6.13), between concentrations ranging from 10.0 - 20.36 μg/g eU and known areas of ore mineralization.

On the map of equivalent thorium concentration (Figure A6.14), these areas are reasonably well defined by concentrations within the range of 20.0 - 49.7 μg/g eTh. Similarly, on the map of eU/K concentration ratio (Figure A6.15), values of 8.0 - 18.0 coincidence well with known mineralization.

These areas also show good correlation with ratio values of 1.0 - 2.3 and higher on the eU/eTh concentration ratio map (Figure A6.16). Ratio values of 12.0 - 27.0 and higher on the eTh/K concentration ratio map (Figure A6.17), show a good coincidence with the known areas of ore mineralization.

(2) Areas of ore mineralization situated outside of the Mole Granite

Most of the known areas of ore mineralization which are located outside the Mole Granite show little correlation with high potassium concentrations (Figure A6.12). This indicates that the mineralization in these areas is not comprised of potassium-rich compounds, such as alteration minerals, e.g. sericite (a variety of mica or muscovite). These areas are poorly delineated by potassium concentrations of 0.5 - 2.5 %.

On the map of equivalent uranium concentration (Figure A6.13), values ranging between 10.0 and 20.36 μg/g eU, show a fairly good to excellent correlation with the known areas of ore mineralization.

On the equivalent thorium concentration map (Figure A6.14), the areas of ore mineralization, in general, coincide with concentrations of 5.0 - 25.0 ug/g eTh. However, these areas are poorly defined by this parameter.

The map of eU/K concentration ratio (Figure A6.15), shows a very close correlation between high ratio values (8.0 - 18.0 and higher) and known areas of ore mineralization. This radiometric parameter shows an improved delineation of local anomalies compared with the other element parameters K, eU, and eTh.

On the map of eU/eTh concentration ratio (Figure A6.16), the areas of ore mineralization generally coincide with patterns representing values of 1.00 - 2.25 and higher.

Patterns with concentration ratio of 12.0 - 27.0 and higher on the map of eTh/K (Figure A6.17), in general, characterize the known areas of ore mineralization in the study area.

6-3 Results from the experimental ground radiometric survey

This section presents results obtained from the experimental ground radiometric investigation. The experiment includes :

- the determination of attenuation factors for the GAD-6/GSP-4 γ-ray spectrometer;
- the ground radiometric surveys at selected traverses in the study area and surrounds; and
- the determination of correlation coefficients between the airborne radiometric data and ground radiometric data.

6-3.1 Experiment for determining the attenuation factors for the GAD-6/GSP-4 γ-ray spectrometer.

The experimental procedure was described in Chapter 4 of this thesis. Figure 6.1 shows the detailed arrangement of the measurement points of the 4 by 4 metre grid. This grid was established on a very large and flat surface of a fresh granite outcrop at the Moonbi Hills road cutting (GR 310 950 mE, 6570 350 mN). Results of the measurements are listed in Tables 6-3.1.1 and 6-3.1.2.

The γ-ray attenuation factors for the GAD-6/GSP-4 spectrometer were calculated using the following formula.

$$N_h = N_0 e^{-\mu h}$$

where

N_h= count rate of γ-ray radiation at height h;

N_0= count rate of γ-ray radiation at ground surface (2π-geometry);

μ= attenuation factor for γ-rays of the relevant energy channel.

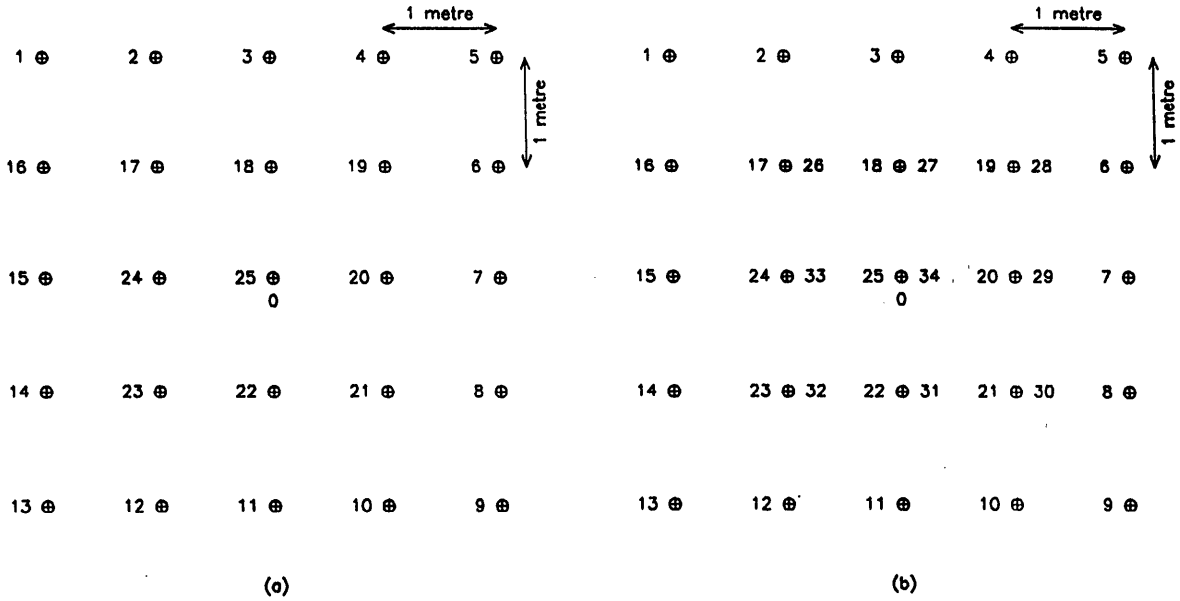

Figure 6.1 Arrangement of the measurement points used in the experiment for determining the attenuation factors for the GAD-6/GSP-4 gamma-ray spectrometer. a) measurement with 2π-geometry; b) measurement with the sensor situated at 800 millimetres above granite surface.

Table 6-3.1.3. lists the attenuation factors for the GAD-6/GSP-4 γ-ray spectrometer obtained from the experiment and used for processing data of the experimental ground radiometric survey.

Table 6-3.1.1
Results of measurements for 2π-geometry

Grid point	TC	K	eU	eTh
		Counts in 100 seconds		
0.00	12744.00	1981.00	736.00	462.00
1.00	12277.00	1993.00	671.00	409.00
2.00	12861.00	1985.00	752.00	470.00
3.00	12748.00	2005.00	735.00	486.00
4.00	12690.00	1989.00	724.00	496.00
5.00	12792.00	1980.00	732.00	480.00
6.00	13125.00	2075.00	759.00	454.00
7.00	13527.00	2056.00	779.00	506.00
8.00	12491.00	1933.00	731.00	458.00
9.00	12432.00	1963.00	674.00	436.00
10.00	12272.00	1930.00	688.00	445.00
11.00	11902.00	1843.00	647.00	457.00
12.00	12310.00	2000.00	619.00	472.00
13.00	12039.00	1942.00	652.00	450.00
14.00	12210.00	1958.00	679.00	425.00
15.00	12178.00	2017.00	635.00	431.00
16.00	12538.00	1988.00	703.00	447.00
17.00	12864.00	2069.00	689.00	471.00
18.00	13156.00	1918.00	777.00	463.00
19.00	13452.00	2147.00	746.00	461.00
20.00	12811.00	1964.00	702.00	462.00
21.00	12358.00	1991.00	715.00	468.00
22.00	12354.00	1948.00	675.00	458.00
23.00	12205.00	1940.00	690.00	477.00
24.00	12968.00	1977.00	722.00	476.00
25.00	12509.00	1966.00	714.00	465.00

Table 6-3.1.2

Results of measurements with sensor head at height 800 millimetres.

Grid point	TC	K	U	Th
	Counts in 100 seconds			
0	10425.0	1616.0	608.0	364.0
1	10165.0	1531.0	511.0	345.0
2	10308.0	1618.0	551.0	353.0
3	10402.0	1618.0	572.0	389.0
4	10248.0	1559.0	595.0	350.0
5	10490.0	1633.0	603.0	373.0
6	10654.0	1608.0	626.0	402.0
7	10519.0	1600.0	617.0	362.0
8	10450.0	1567.0	591.0	400.0
9	10452.0	1644.0	568.0	391.0
10	10312.0	1588.0	561.0	389.0
11	10053.0	1578.0	531.0	374.0
12	10092.0	1574.0	559.0	385.0
13	10093.0	1583.0	546.0	391.0
14	10211.0	1617.0	567.0	392.0
15	10375.0	1571.0	548.0	375.0
16	10097.0	1611.0	549.0	359.0
17	10516.0	1600.0	551.0	369.0
18	9867.0	1495.0	558.0	335.0
19	10695.0	1693.0	647.0	377.0
20	10308.0	1532.0	538.0	403.0
21	10707.0	1602.0	576.0	352.0
22	10087.0	1573.0	563.0	362.0
23	10832.0	1697.0	600.0	407.0
24	10120.0	1608.0	582.0	363.0
25	10916.0	1674.0	570.0	387.0
26	10052.0	1628.0	572.0	357.0
27	10616.0	1622.0	622.0	379.0
28	10056.0	1570.0	541.0	359.0
29	10487.0	1611.0	586.0	364.0
30	10036.0	1568.0	573.0	359.0
31	10429.0	1627.0	606.0	379.0
32	10020.0	1531.0	518.0	374.0
33	10700.0	1559.0	605.0	394.0
34	10013.0	1584.0	554.0	329.0

Table 6-3.1.3
Attenuation factors of γ-rays for the GAD-6/GSP-4 spectrometer

Radioelements	Energy window (MeV)	Attenuation factor m^{-1}
Th	2.41 - 2.81	0.266
U	1.62 - 1.87	0.259
K	1.37 - 1.57	0.284
TC	0.40 - 3.0	0.247

6-3.2 The experimental ground radiometric survey

This section describes the results obtained from the experimental ground radiometric investigation at selected traverses within the study area and surrounds.

Radiometric profiles of total radiation counts (TC), potassium concentration (K), equivalent uranium concentration (eU), and equivalent thorium concentration (eTh) for each survey line are presented in Appendix volume of this thesis. Profiles of ratio parameters such as eU/K, eU/eTh, and eTh/K are also presented.

The Silent Grove radiometric survey (Line RR-01)

This survey line extends for about 42 kilometres, starting from near Glen Creek (GR 372 900 mE, 6748 600 mN) and terminating at Silent Grove (GR 369 500 mE, 6778 900 mN). Figure A6.18 shows the radiometric profiles obtained from the survey. Three types of principal rock units were encountered along the survey line. These were :

- the Tent Hill Porphyrite;
- the Mole Granite; and
- the Permo-Carboniferous sedimentary rocks.

The radiometric response of the Tent Hill Porphyrite

The Tent Hill Porphyrite is characterized by:

(a) total radiation count, 40 - 80 cps.

(b) potassium concentration, less than 3.5 %.

(c) equivalent uranium concentration, 1.0 - 4.0 μg/g eU.

(d) equivalent thorium concentration, 10.0 - 20.0 μg/g eTh.

(e) eU/K ratio, less than 2.0.

(f) eU/eTh ratio, 0.05 - 0.25.

(g) eTh/K ratio, 8.0 - 12.0.

The radiometric response of the Mole Granite

(a) total radiation count. Levels as high as 175 cps characterize the outcropped body of the Mole Granite. Variation in the radiation intensities is mostly caused by variation in the thickness and extent of the soil cover which provides a masking effect to the granite surface. A low radiation count rate within the range of 50 - 60 cps was recorded on the Torrington Roof Pendant. This low radiation level originated from the sedimentary rocks which form the roof pendant.

(b) potassium concentration, 1.0 - 4.0 %.

(c) equivalent uranium concentration, 3.0 - 15.0 μg/g eU.

(d) equivalent thorium concentration. 10.0 - 70.0 μg/g eTh.

(e) eU/K ratio, 2.0 - 4.0.

(f) eU/eTh ratio, 0.1 - 0.5.

(g) eTh/K ratio, 5.0 - 30.0.

The radiometric response of the Permo-Carboniferous sedimentary rocks

These units are characterized by:

(a) total radiation count, 10 - 30 cps.

(b) potassium concentration, 1.0 - 2.0 %.

(c) equivalent uranium concentration, 1.0 - 3.0 μg/g eU.

(d) equivalent thorium concentration, approximately 10.0 μg/g eTh.

(e) eU/K ratio, 0.5 - 1.0.

(f) eU/eTh ratio, less than 0.25.

(g) eTh/K ratio, 5.0 - 7.0.

The Torrington radiometric survey (Line RR-02)

A five-kilometre traverse was surveyed for the Torrington radiometric investigation. Figure A6.19 shows the results of the survey. Two principal rock units were recognized in this survey line, the Adamellite and the Mole Granite.

Radiometric response of the Adamellite

This Adamellite is known to be an I-type intrusive rock. It outcrops in an area situated about 2 kilometres to the east of Torrington. Only minor outcrops were found in the area where the survey started.

This unit is characterized by:

(a) total radiation count, 50 - 60 cps.

(b) potassium concentration, 2.0 - 3.0 %.

(c) equivalent uranium concentration, less than 2.0 μg/g eU.

(d) equivalent thorium concentration, 5.0 - 10.0 μg/g eTh.

(e) eU/K ratio, 0.5 - 1.0.

(f) eU/eTh ratio, 0.15 - 0.2.

(g) eTh/K ratio, 2.0 - 4.0

The radiometric response of the Mole granite

In this area the Mole Granite is characterized by:

(a) total radiation count, 50 - 120 cps. Variation in the radiation level was caused chiefly by variation in the thickness of the granite-derived soil which covers the parent rock, producing a masking effect which attenuates the γ-ray emitted from the surface of the granite. A similar effect can also be seen on the radioelement concentration profiles K, eU, and eTh.

(b) potassium concentration, 1.0 - 3.5 %.

(c) equivalent uranium concentration, 1.5 - 7.0 μg/g eU.

(d) equivalent thorium concentration, 8.0 - 42.0 μg/g eTh.

(e) eU/K ratio, 0.75 - 2.0.

(f) eU/eTh ratio, less than 0.2.

(g) eTh/K ratio, 5.0 - 14.0

The Oaky Creek radiometric survey (Line RR-03)

This survey line extends for about 6 kilometres, starts from near the Roma Valley Homestead (GR 375 400 mE, 6769 000 mN), crosses the Oaky Creek, and terminates near the Sugarloaf High Peak (GR 379 700 mE, 6766 000 mN). The survey covered two major rock types, the alluvial sediments and the Mole granite. Figure A6.20 depicts the results of the survey.

The radiometric response of the alluvial sediments

These alluvial sediments occupy a wide valley where the Oaky Creek flows. The sediments in this area are characterized by:

(a) total radiation count, 50 - 60 cps.

(b) potassium concentration, 2.0 - 3.0 %.

(c) equivalent uranium concentration, 2.0 - 4.0 μg/g eU.

(d) equivalent thorium concentration, 10.0 - 15.0 μg/g eTh.

(e) eU/K ratio, 0.5 - 1.0.

(f) eU/eTh ratio, less than 0.3.

(g) eTh/K ratio, 4.0 - 5.0.

The radiometric response of the Mole Granite

In this area, the Mole Granite is characterized by:

(a) total radiation count, 80 - 160 cps.

(b) potassium concentration, 3.0 - 4.0 %.

(c) equivalent uranium concentration, 2.0 - 12.0 μg/g eU.

(d) equivalent thorium concentration, 20.0 - 65.0 μg/g eTh.

(e) eU/K ratio, 1.0 - 3.0.

(f) eU/eTh ratio, less than 0.20.

(g) eTh/K ratio, 4.0 - 17.0.

The Pyes Creek radiometric survey (Line RR-04)

A six-kilometre survey line was traversed in this area. Figure A6.21 shows the results obtained. Three principal rock units were encountered in the investigation, the Mole Granite, the Permian Volcanic rock, and the Pyes Creek Leuco-Adamellite.

The radiometric response of the Mole Granite

In this survey area, the Mole Granite is characterized by:

(a) total radiation count, 50 - 120 cps.

(b) potassium concentration, 2.0 - 4.0 %.

(c) equivalent uranium concentration, 4.0 - 8.0 μg/g eU.

(d) equivalent thorium concentration, 10.0 - 40.0 μg/g eTh.

(e) eU/K ratio, 1.5 - 2.5.

(f) eU/eTh ratio, less than 0.25.

(g) eTh/K ratio, 5.0 - 12.0.

The Wellington Vale radiometric survey (Line RR-05)

This survey line extends for about eight kilometres. It starts from Glen Leigh (GR

375 800 mE, 6744 600 mN) and terminates at the road juction situated 1.3 kilometres to the north-east-east of the Wangi-Wangi homestead (GR 382 700 mE, 6743 500 mN). The survey mainly traversed the Dundee Rhyodacite. A minor alluvial sedimentary unit was also encountered. Figure A6.22 presents the results of the survey.

In this survey line, the Dundee Rhyodacite is characterized by:

(a) total radiation count, 30 - 50 cps. A drop in radiation level of 15.0 cps. was recorded when the survey passed over the alluvial sediments.

(b) potassium concentration, 1.0 - 2.0 %.

(c) equivalent uranium concentration, 1.0 - 3.0. μg/g eU.

(d) equivalent thorium concentration, 7.0 - 13.0 μg/g eTh.

(e) eU/K ratio, 0.5 - 1.5.

(f) eU/eTh ratio, less than 0.25.

(g) eTh/K ratio, 5.0 - 7.0.

The Beardy River radiometric survey (Line RR-06)

The Beardy River radiometric survey covers a distance of 4 kilometres. It starts from the cliff near the river (GR 355 400 mE, 6755 900 mN). The survey was mainly conducted on the Permo-Carboniferous rocks. Figure A6.23 shows the results obtained from the survey.

The sedimentary rocks in this area are indicated by:

(a) total radiation count, 40 - 60 cps. Variation in the radiation intensity was caused mainly by a change in the soil thickness and extent in the area.

(b) potassium concentration, less than 3.0 %.

(c) equivalent uranium concentration, 1.0 - 2.5. μg/g eU.

(d) equivalent thorium concentration, 10.0 - 15.0 μg/g eTh.

(e) eU/K ratio, 0.75 - 1.5.

(f) eU/eTh ratio, less than 0.3.

(g) eTh/K ratio, 5.0 - 7.0.

The Bolivia Range radiometric survey (Line RR-07)

The Bolivia Range radiometric survey line extends for about 14 kilometres, starting from near Rockdale (GR 392 600 mE, 6749 050 mN) and terminating near the Hollywood homestead (GR 399 400 mE, 6759 400 mN). Three types of principal rock units were encountered in the survey, the Permian Volcanic unit, the Bolivia Range Leuco-Adamellite, and the Bolivia mass. Results of the survey are presented in Figure A6.24.

The radiometric response of the Permian Volcanic unit

The volcanic rock in this area is composed mainly of acid-to-intermediate eruptives with minor interbedded sediments (Brunker and Chesnut, 1976). This rock is characterized by:

(a) total radiation count, approximately 50 cps.

(b) potassium concentration, 2.0 - 3.0 %.

(c) equivalent uranium concentration, less than 2.5 μg/g eU.

(d) equivalent thorium concentration, approximately 20.0 μg/g eTh.

(e) eU/K ratio, less than 2.0.

(f) eU/eTh ratio, less than 0.2.

(g) eTh/K ratio, 7.0 - 8.0.

The radiometric response of the Bolivia Range Leuco-Adamellite

The adamellite in this area is indicated by:

(a) total radiation count, 60 - 140 cps.

(b) potassium concentration, 2.0 - 3.5 %.

(c) equivalent uranium concentration, 2.5 - 7.5 μg/g eU.

(d) equivalent thorium concentration, 20.0 - 40.0 μg/g eTh.

(e) eU/K ratio, 1.0 - 2.5.

(f) eU/eTh ratio, 0.1 - 0.3.

(g) eTh/K ratio, 8.0 - 14.0.

The radiometric response of the Bolivia mass

The Bolivia mass is characterized by:

(a) total radiation count, approximately 50 cps.

(b) potassium concentration, approximately 2.0 %.

(c) equivalent uranium concentration, 1.0 - 3.0 μg/g eU.

(d) equivalent thorium concentration, 10.0 - 18.0 μg/g eTh.

(e) eU/K ratio, 0.5 - 1.5.

(f) eU/eTh ratio, less than 0.2.

(g) eTh/K ratio, 4.0 - 8.0.

6-3.3 Analysis of the correlation coefficients of the experimental ground radiometric data and the airborne radiometric data

A simple linear regression analysis was used to determine the correlation coefficients between the experimental ground radiometric data and airborne radiometric data. The MINITAB Statistics Package on the DEC-20R Computer System was utilized in the analysis. This analysis provides conversion factors which were used for transforming the normalized count rate of the airborne radiometric data into elemental concentrations. The analysis was only made for the Silent Grove Road experimental ground radiometric survey because the survey line is situated in the centre of the area and it provided sufficient data for such an analysis.

Tables 6-3.3.1., 6-3.3.2.. 6-3.3.3. show the isolated data pairs of the airborne and experimental ground radiometric data. The procedure for isolating the data pairs, which involves sorting and searching of particular pairs of data, is described in Chapter 5 of this thesis. Results of the analysis appear in the same tables. Illustrations of the analysis are depicted in Figures 6.2, 6.3, and 6.4.

Table 6-3.3.1
Results of analysis of isolated data pairs in potassium channel

Data point	Normalized count	Concentration
1	107.36	2.43
2	118.07	2.71
3	90.71	2.35
4	167.33	3.62
5	200.25	4.12
6	114.39	2.07
7	90.27	1.34
8	90.69	0.64
9	53.16	0.54
10	89.27	1.01
11	140.50	2.38
12	177.04	3.41
13	160.92	3.36
14	147.53	3.76
15	178.99	2.67
16	141.45	2.42
17	131.07	2.32
18	107.65	1.92
19	91.95	1.19
20	92.05	1.79

Table 6-3.3.2
Results of analysis of isolated data pairs in uranium channel

Data point	Normalized count	Concentration
1	12.89	1.27
2	15.18	1.69
3	13.22	2.23
4	35.34	7.87
5	36.14	7.67
6	29.08	5.21
7	17.23	3.52
8	12.35	2.29
9	13.62	3.01
10	20.90	4.45
11	18.35	3.46
12	27.57	7.32
13	25.30	6.58
14	34.57	9.85
15	24.02	5.14
16	9.98	4.12
17	17.19	3.18
18	16.35	1.87
19	9.48	1.31
20	6.24	0.80

Table 6-3.3.3
Results of analysis of isolated data pairs in thorium channel

Data point	Normalized count	Concentration
1	17.00	14.97
2	31.85	23.30
3	28.81	14.71
4	117.37	56.75
5	111.15	49.24
6	52.76	26.16
7	35.38	12.97
8	46.08	10.91
9	30.61	9.19
10	37.88	24.88
11	47.02	22.17
12	71.40	36.98
13	60.12	33.19
14	90.90	44.22
15	93.46	34.38
16	82.86	38.30
17	62.35	21.36
18	37.37	20.50
19	6.50	8.18
20	10.93	8.16

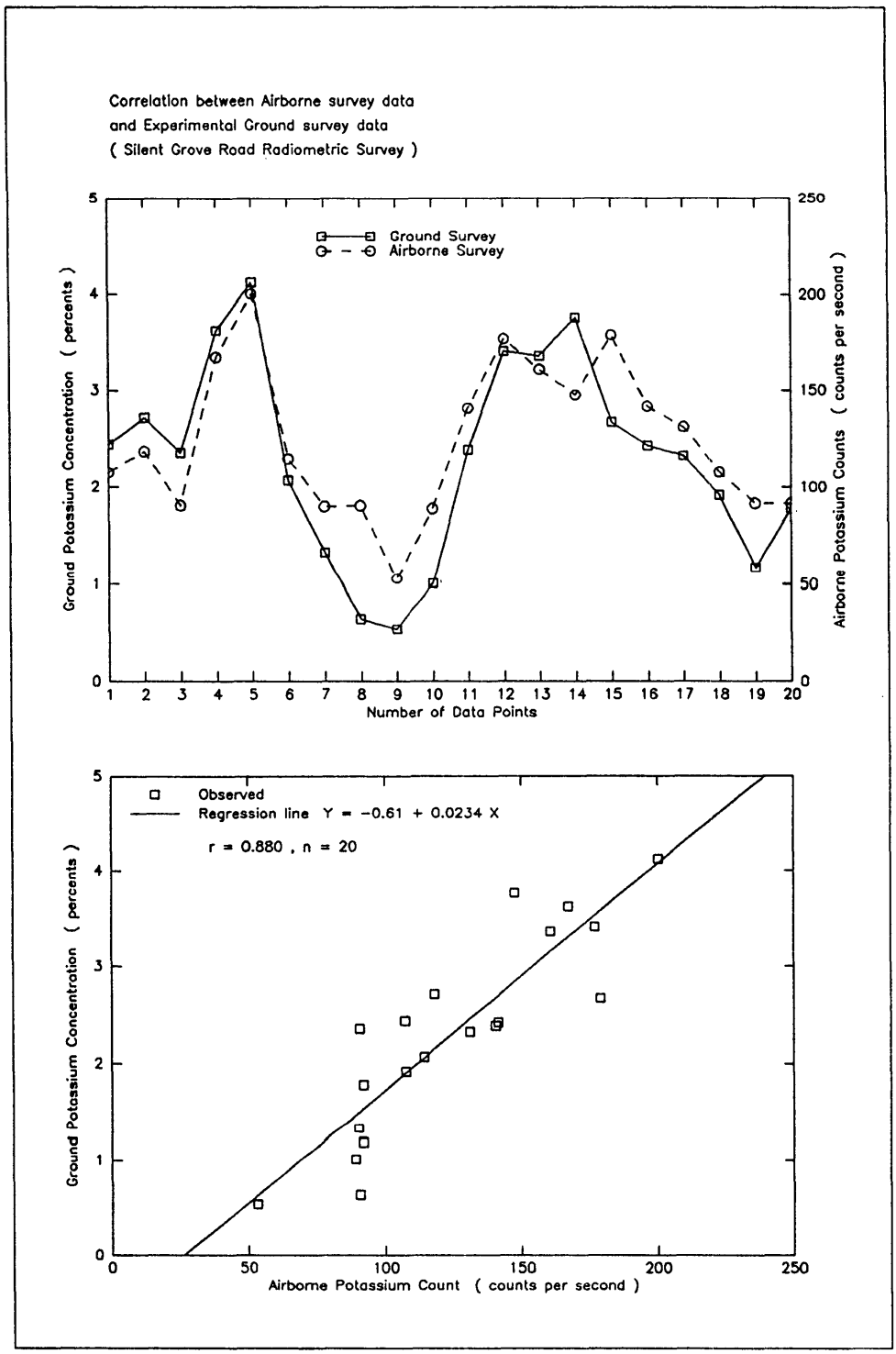

Figure 6.2 Correlation analysis of isolated data pairs of normalized count rate of the airborne and experimental ground radiometric survey. (Potassium channel).

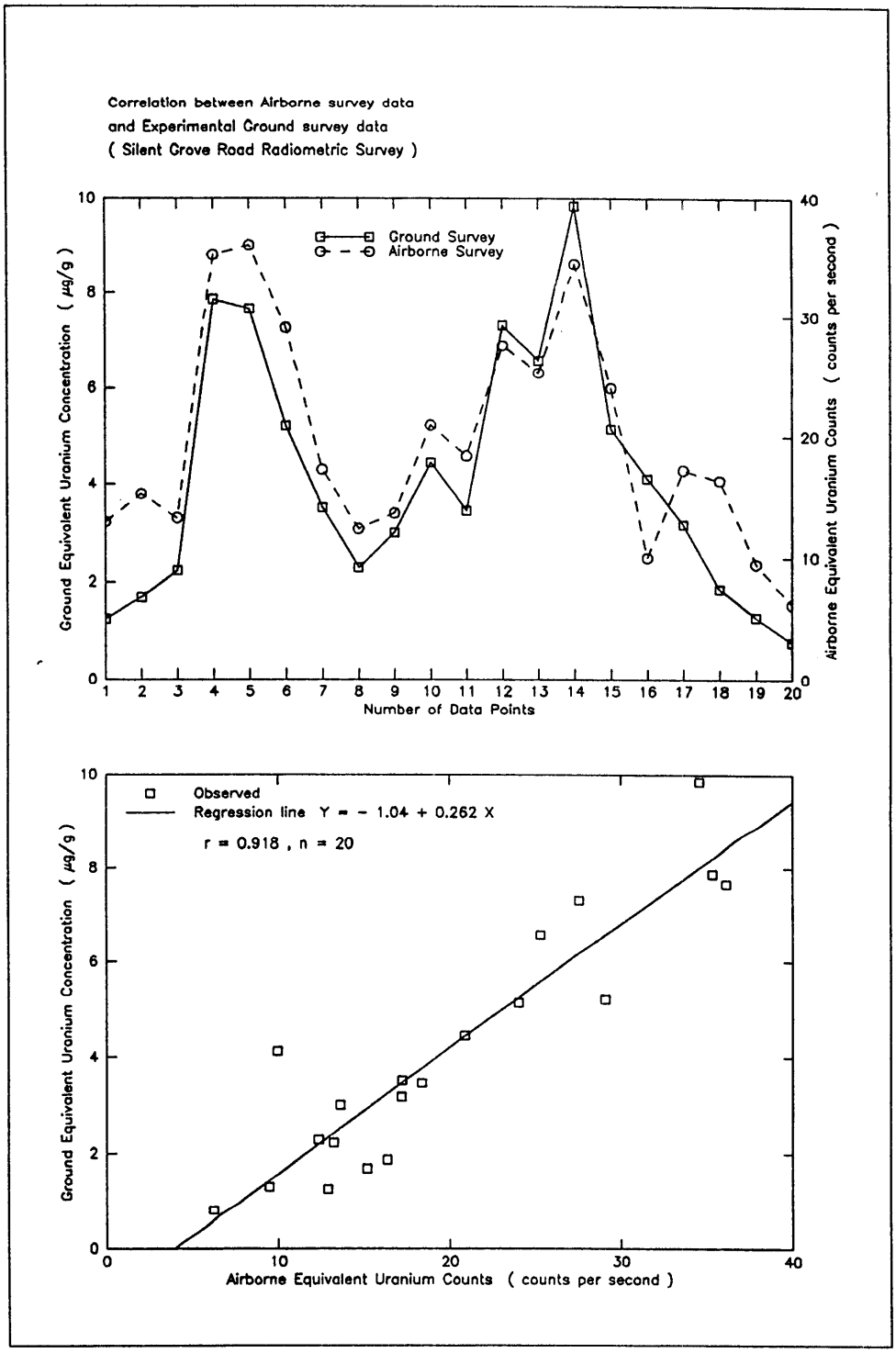

Figure 6.3 Correlation analysis of isolated data pairs of normalized count rate of the airborne and experimental ground radiometric survey. (Uranium channel).

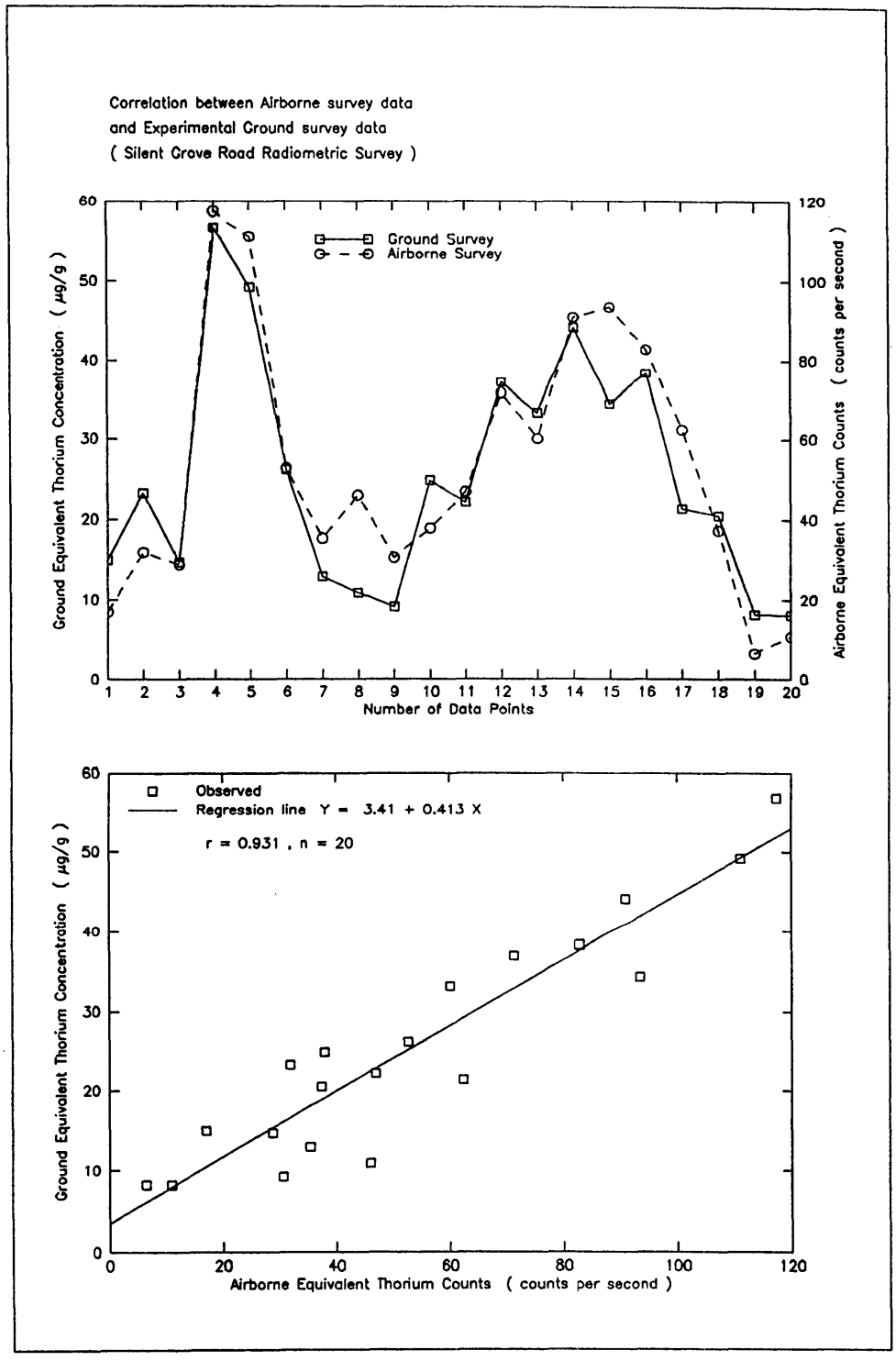

Figure 6.4 Correlation analysis of isolated data pairs of normalized count rate of the airborne and experimental ground radiometric survey. (Thorium channel).

6-4 Results from the laboratory γ-ray spectrometric analysis

This section presents the results of the laboratory γ-ray spectrometric analysis of rock specimens collected in the study area and surrounds.

Based on the international standard rock samples GSP-1, G-2, AGV-1, and BCR-1, with known concentrations of uranium and thorium, the analysis determines concentration of those radioelements in other rocks samples. Figures 6.5 - 6.8 show the spectral characteristics and other pertinent data of the standard rocks mentioned above. The stripping factor in the uranium window due to the interference from the γ-ray photons in the thorium channel was evaluated from the GSP-1 and G-2 standard specimens. Figures 6.9 and 6.10 depict the standardization curves for determining the concentration of uranium and thorium. The standardization was performed using the GSP-1, G-2, and AGV-1 samples. The BCR-1 specimen was ignored due to its high iron content, for which a mass absorption coefficient for correcting the count rate would be necessary (Enders, 1984).

Tables 6-4.1(a) and 6-4.1(b) list the concentration of equivalent uranium* and equivalent thorium in the rock samples acquired from several locations in the study area and its vicinity. Potassium concentration was not evaluated due to the lack of standardization.

Table 6-4.2 shows results of major-element analysis from rocks gathered from some tin-mining locations in the study area.

Table 6-4.3 lists results of trace-element analysis from some of the rocks listed in Table 6-4.2.

---

*A number of analytical values for eU can only be made using a significant extrapolation of the calibration curve. This has been cross checked by Enders (1984) and found to be satisfactory when compared with analyses by other methods (delayed neutron analysis).

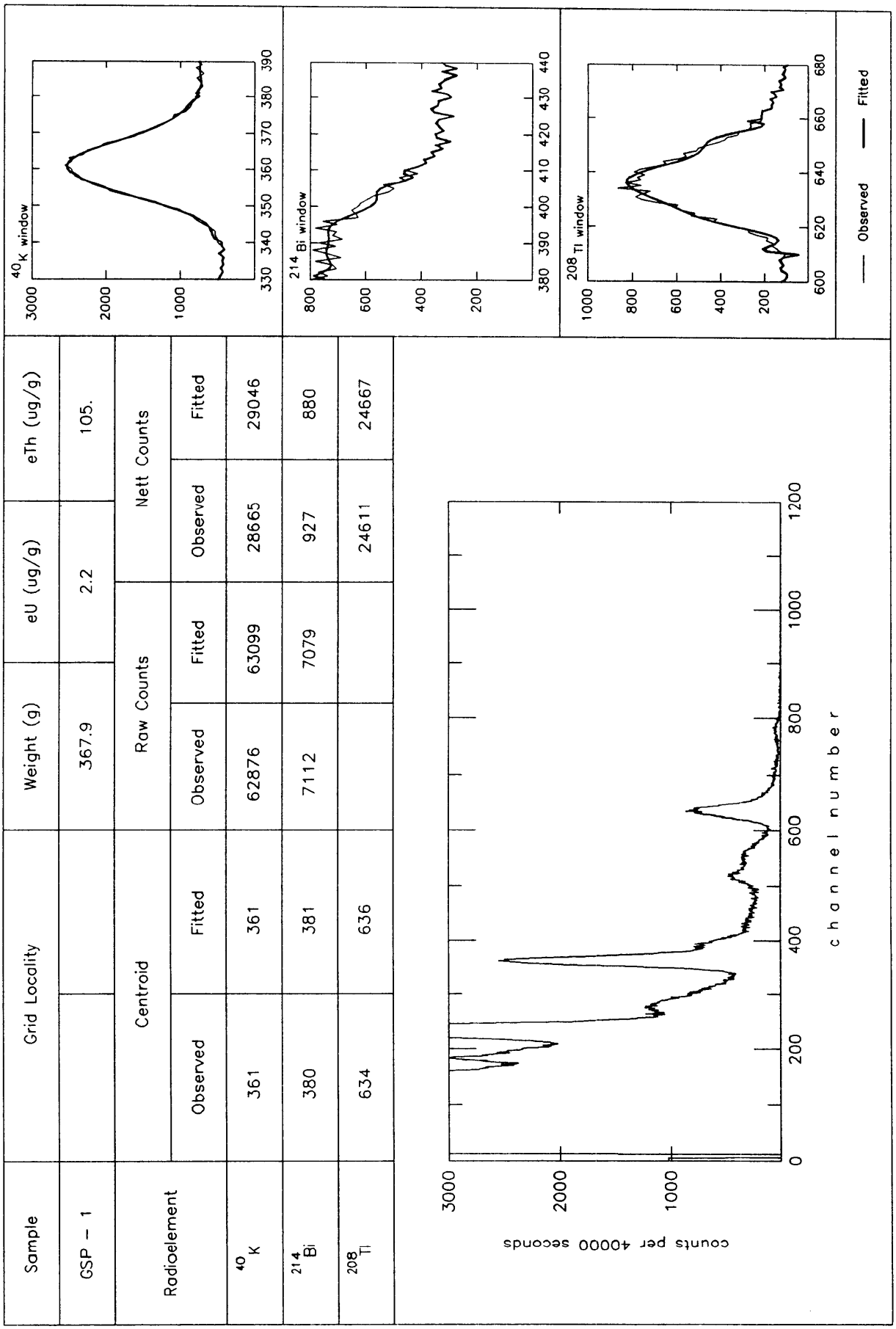

Sample	Grid Locality	Weight (g)	eU (ug/g)	eTh (ug/g)
GSP – 1		367.9	2.2	105.

Radioelement	Centroid		Raw Counts		Nett Counts	
	Observed	Fitted	Observed	Fitted	Observed	Fitted
^{40}K	361	361	62876	63099	28665	29046
^{214}Bi	380	381	7112	7079	927	880
^{208}Tl	634	636			24611	24667

Figure 6.5 Spectral characteristic of standard rock sample GSP-1 and its pertinent data.

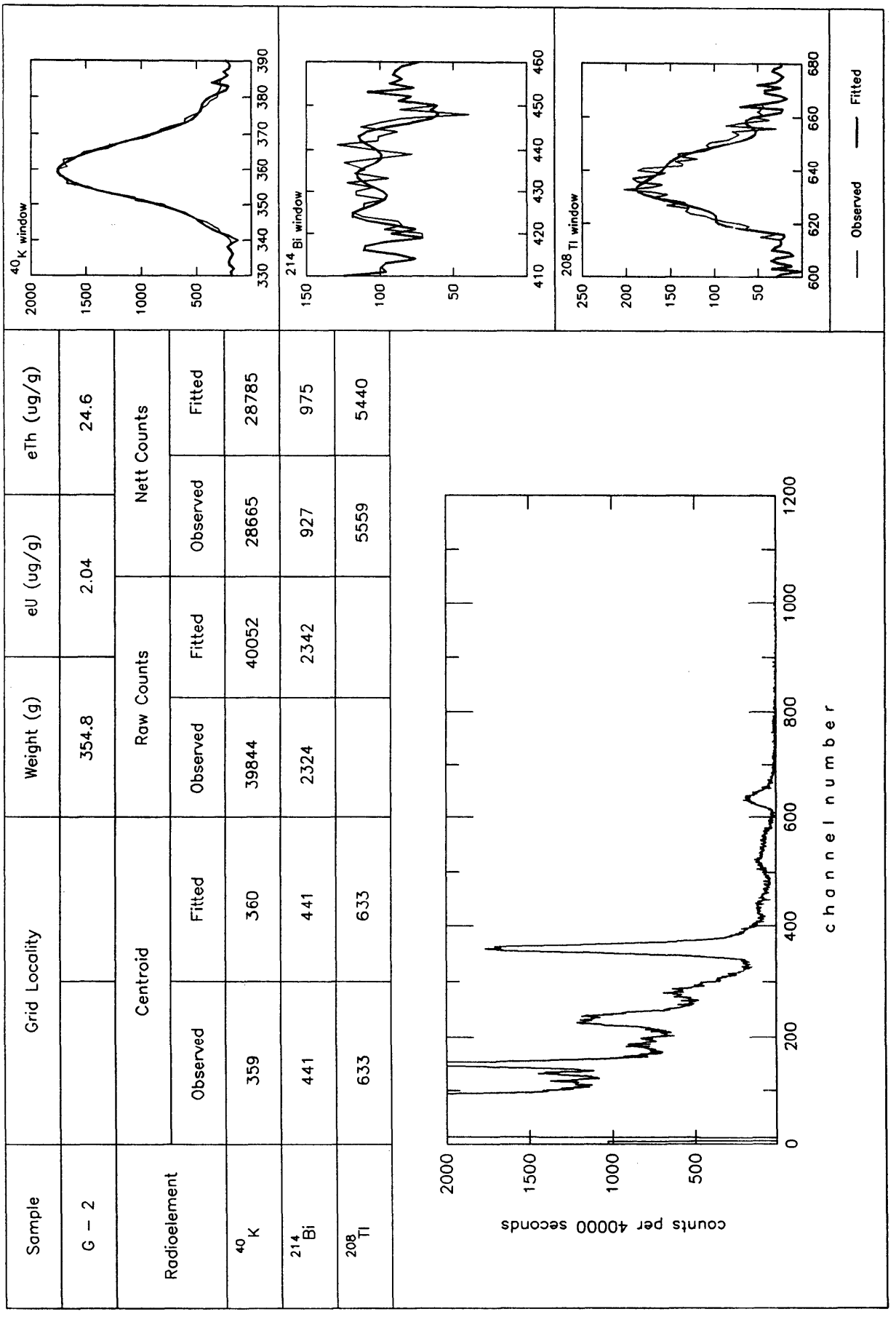

Sample	Grid Locality		Weight (g)	eU (ug/g)	eTh (ug/g)
G – 2			354.8	2.04	24.6

Radioelement	Centroid		Raw Counts		Nett Counts	
	Observed	Fitted	Observed	Fitted	Observed	Fitted
^{40}K	359	360	39844	40052	28665	28785
^{214}Bi	441	441	2324	2342	927	975
^{208}Tl	633	633			5559	5440

Figure 6.6 Spectral characteristic of standard rock sample G-2 and its pertinent data.

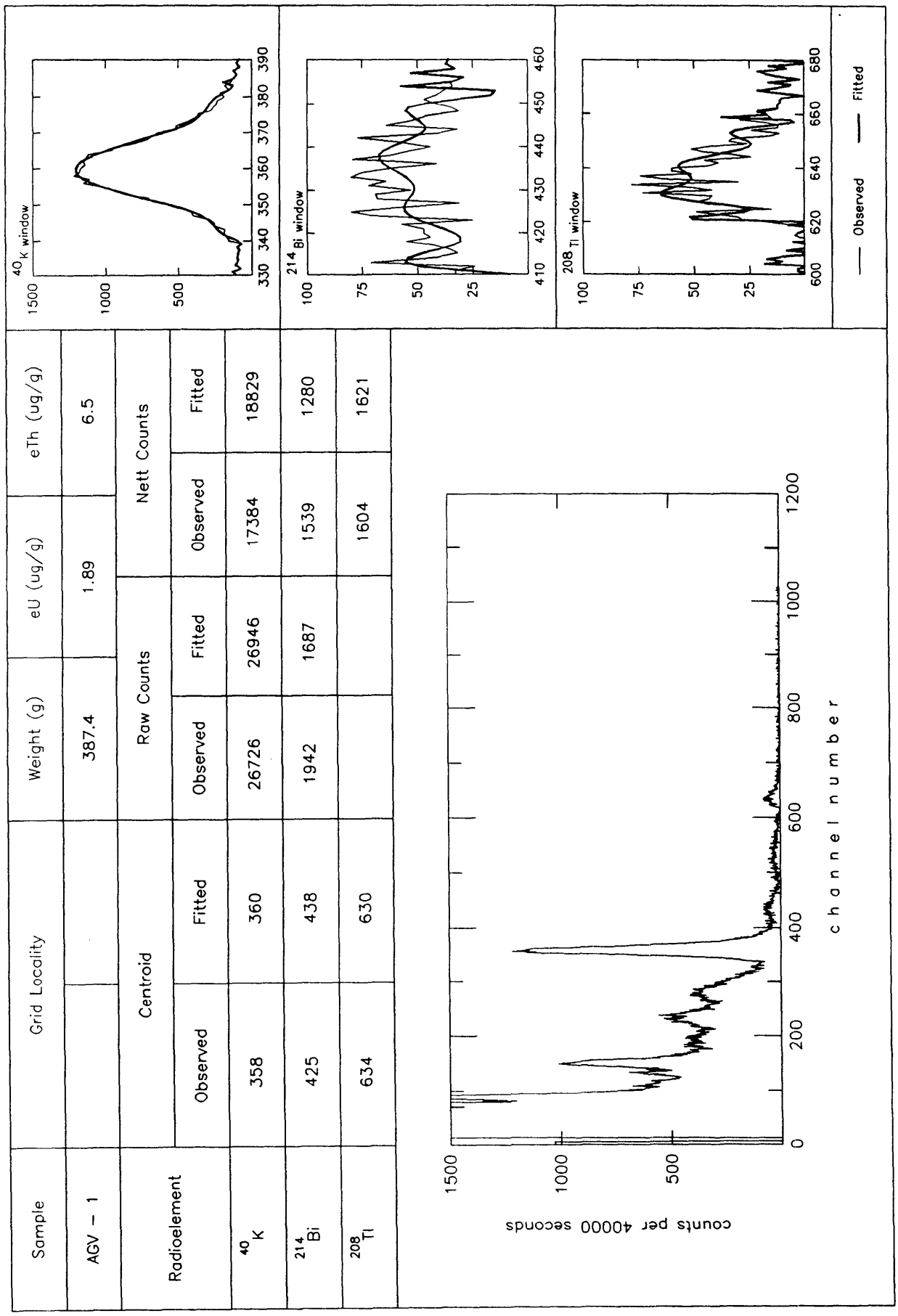

Sample	Grid Locality	Weight (g)	eU (ug/g)	eTh (ug/g)
AGV – 1		387.4	1.89	6.5

Radioelement	Centroid		Raw Counts		Nett Counts	
	Observed	Fitted	Observed	Fitted	Observed	Fitted
^{40}K	358	360	26726	26946	17384	18829
^{214}Bi	425	438	1942	1687	1539	1280
^{208}Tl	634	630			1604	1621

Figure 6.7 Spectral characteristic of standard rock sample AGV-1 and its pertinent data.

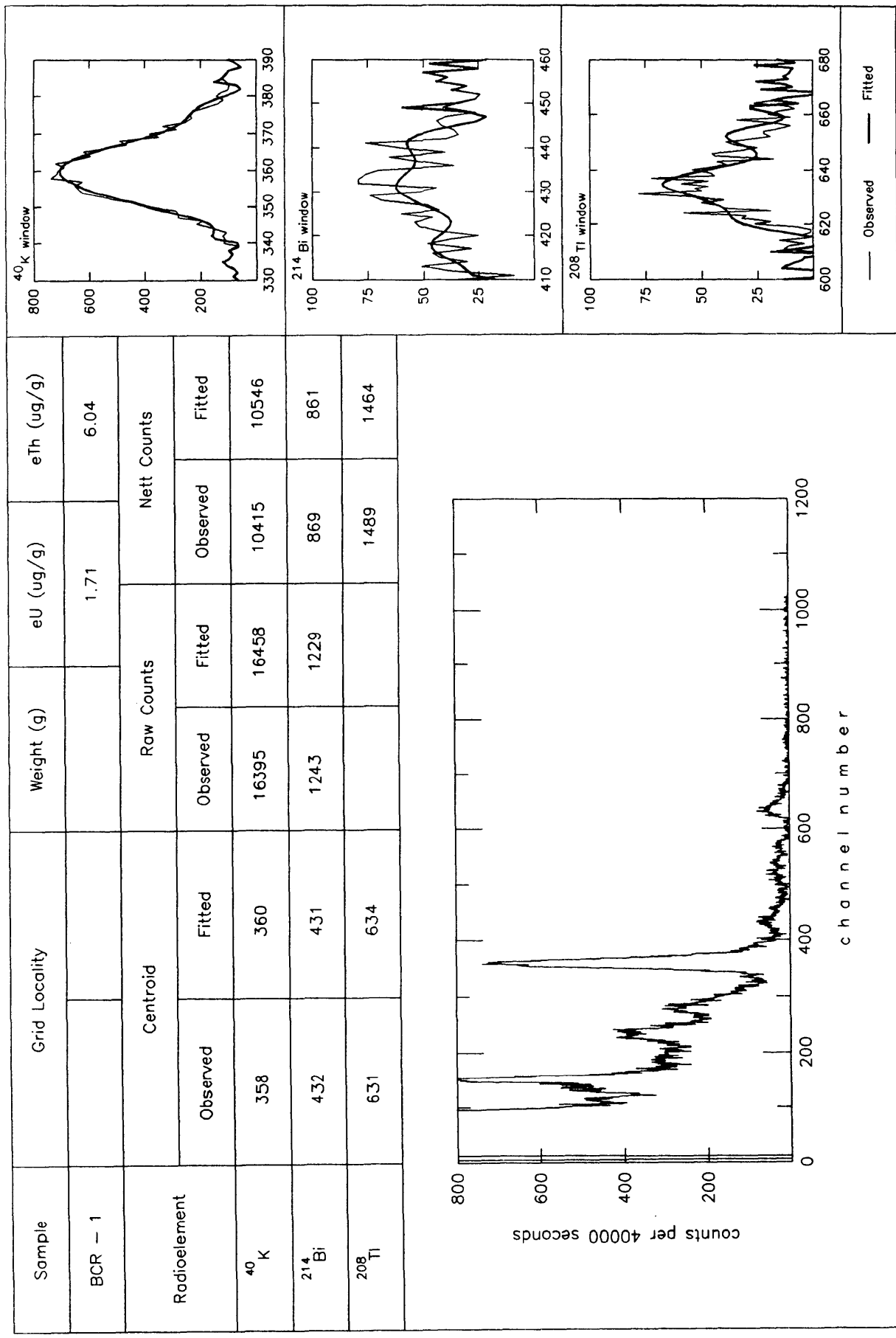

Sample	Grid Locality		Weight (g)	eU (ug/g)	eTh (ug/g)
BCR – 1				1.71	6.04

Radioelement	Centroid		Raw Counts		Nett Counts	
	Observed	Fitted	Observed	Fitted	Observed	Fitted
^{40}K	358	360	16395	16458	10415	10546
^{214}Bi	432	431	1243	1229	869	861
^{208}Tl	631	634			1489	1464

Figure 6.8 Spectral characteristic of standard rock sample BCR-1 and its pertinent data.

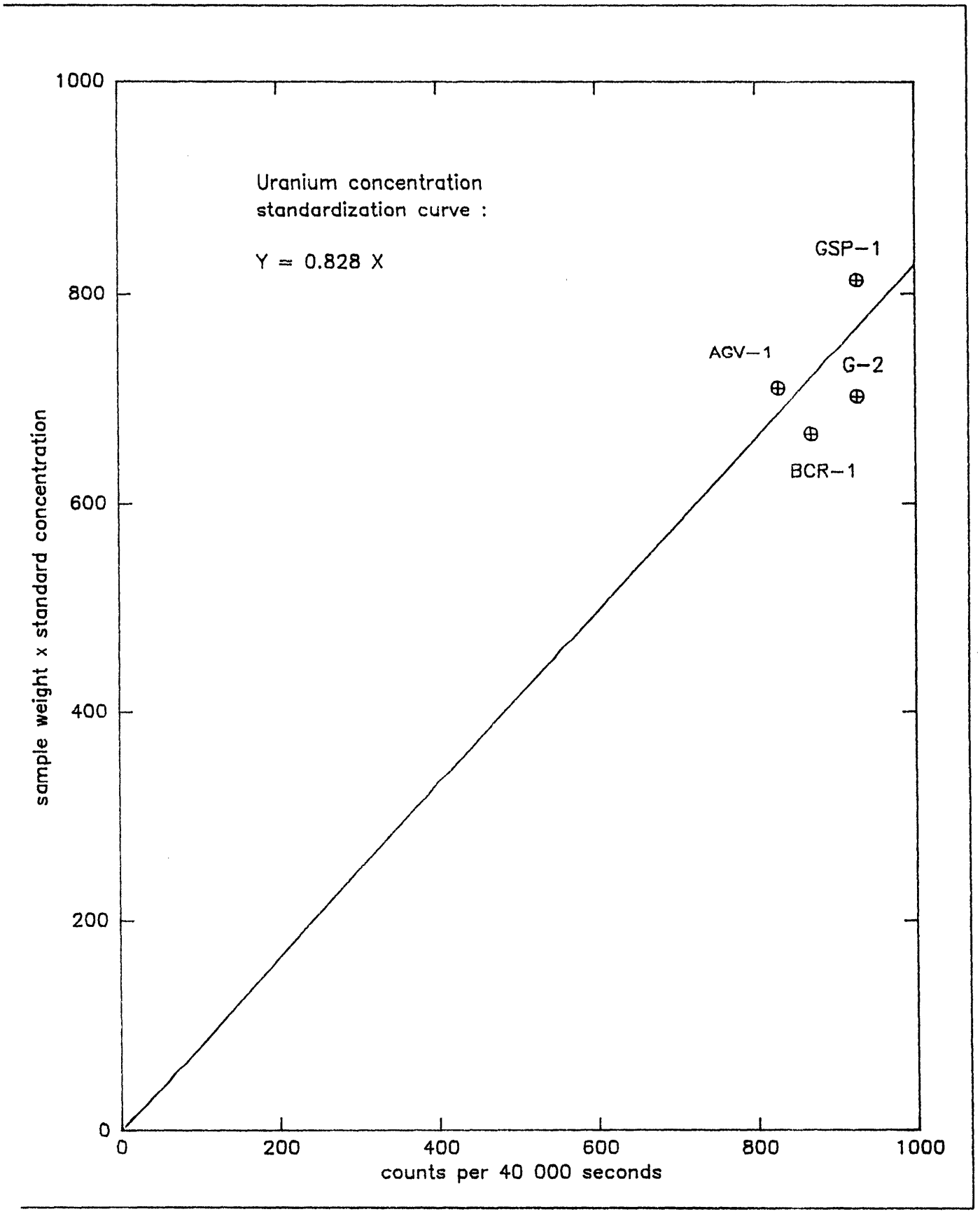

Figure 6.9 Standardization curve for determining uranium concentration based on the standard rocks GSP-1, G-2, and AGV-1.

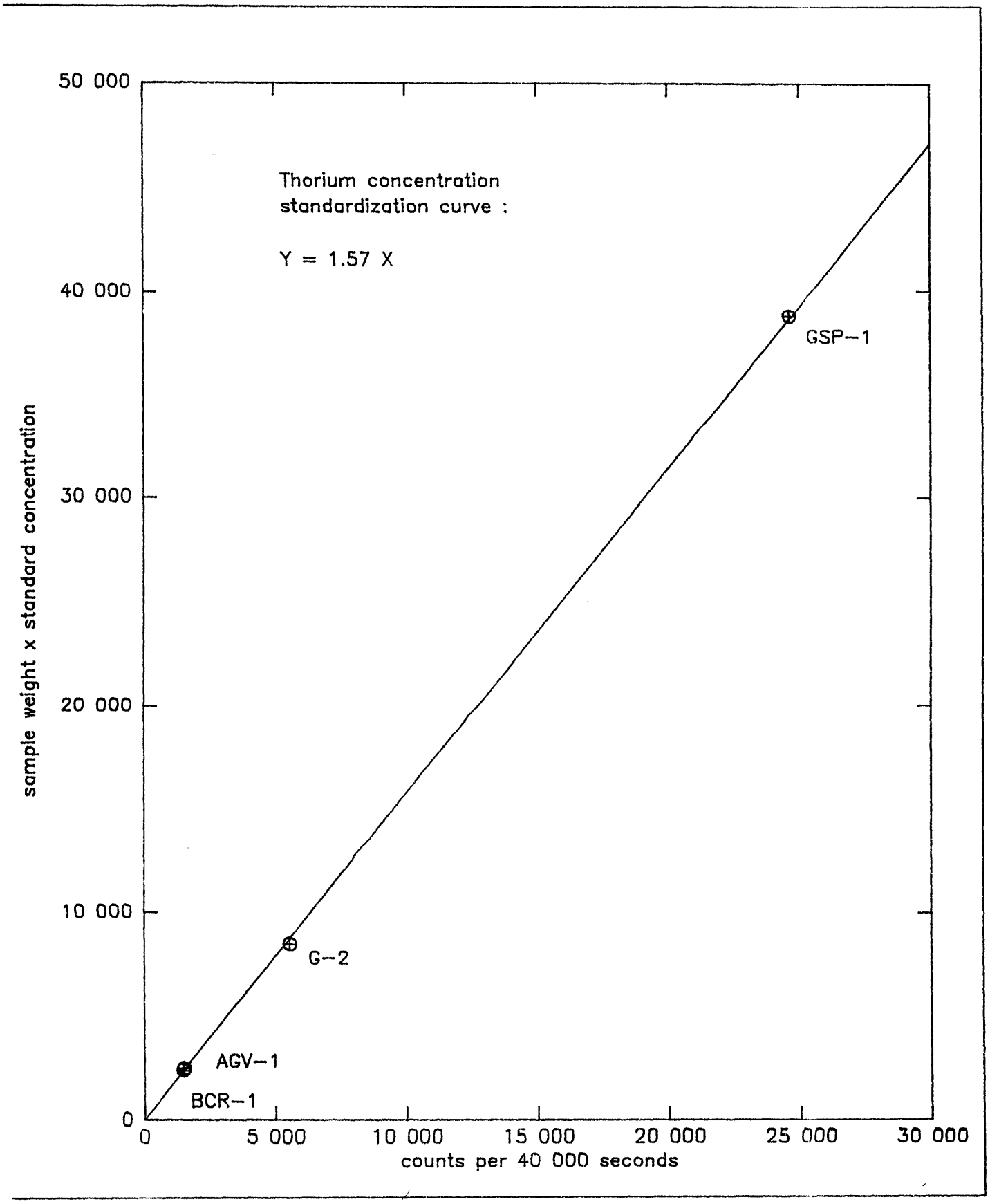

Figure 6.10 Standardization curve for determining thorium concentration based on the standard rocks GSP-1, G-2, and AGV-1.

Table 6-4.1(a) Equivalent uranium and equivalent thorium concentration of rock samples collected within the study area and surrounds.

Sample	Grid Locality	eU(ug/g)	eTh(ug/g)
SGR-01	373150 mE; 6772650 mN	25.17	44.64
SGR-02	372200 mE; 6768150 mN	8.11	44.82
SGR-03	372750 mE; 6767650 mN	17.59	30.82
SGR-04	372800 mE; 6755750 mN	10.39	44.13
SGR-05	371900 mE; 6763200 mN	28.55	31.41
SGR-06	374900 mE; 6752750 mN	16.36	30.66
SGR-07	373100 mE; 6767100 mN	10.02	24.07
SGR-08	373200 mE; 6772900 mN	4.23	6.66
GBM-01	367200 mE; 6742750 mN	8.49	19.51
MBI-01	310950 mE; 6570350 mN	16.43	27.47
BDY-01	355500 mE; 6755400 mN	6.25	21.16
TOR-01	376950 mE; 6758900 mN	1.98	35.20
WEL-01	381600 mE; 6743100 mN	6.63	13.22
WEL-02	381500 mE; 6743200 mN	5.93	11.89
WEL-03	375850 mE; 6744600 mN	6.86	12.77
PYS-01	383850 mE; 6760900 mN	13.06	32.52
PYS-02	384400 mE; 6760850 mN	4.97	13.65
PYS-03	386000 mE; 6760600 mN	12.66	34.51
PYS-04	386000 mE; 6760650 mN	18.79	42.53
PYS-05	386750 mE; 6760700 mN	11.75	35.47
PYS-06	387150 mE; 6760600 mN	14.61	35.45
PYS-07	380600 mE; 6761450 mN	10.71	28.58
BOL-01	396800 mE; 6757250 mN	4.94	14.42
BOL-02	394750 mE; 6755350 mN	15.72	39.13
BOL-03	393400 mE; 6754500 mN	12.45	27.03
BOL-04	393150 mE; 6750700 mN	7.59	15.68

**) Rock samples collected from within study area during the experimental ground radiometric survey.

Table 6-4.1(b) Equivalent uranium and equivalent thorium concentration of rock samples collected within the study area and surrounds. (Rock samples supplied by Brodie (1983)).

Sample	Grid Reference	General Description	eU(ug/g)	eTh(ug/g)
		Mole Granite		
R545531	764692	microgranite type	30.64	34.18
R545532	768691	microgranite type	13.29	45.76
R545533	763694	microgranite type	23.59	53.43
R545536	761692	porphyritic variant	18.93	36.55
R545537	758696	porphyritic variant	19.48	31.39
R545538	759694	porphyritic variant	20.82	30.84
R545542	715691	coarse-grained type	18.14	36.51
R545543	719690	coarse-grained type	12.41	44.62
R545544	718698	coarse-grained type	36.53	42.68
R545551	745749	Gibraltar Ignimbrite basal layer	7.87	18.58
R545568	715736	Silent Grove Mine quartz-sericite-chlorite alteration	36.73	40.68
R545570	715736	silicic alteration ore zone	29.14	37.75
R545579	705746	McDowells Contact Lode quartz-sericite-chlorite alteration	31.16	40.30
R545585	705746	ore zone	31.17	49.06

*) Rock samples supplied by Brodie (1983).

Table 6-4.2 Major element analysis of rock samples acquired from some tin mines in the study area. (Supplied by Kleeman (1985); Unpublished data).

	(172) 366000 mE 6754000 mN	(180) 372000 mE 6756500 mN	(182) 375500 mE 6757000 mN	(189) 372000 mE 6774000 mN	(191) 370750 mE 6774500 mN
SiO_2	76.50	77.10	67.21	76.84	76.12
TiO_2	0.09	0.14	0.50	0.08	0.06
Al_2O_3	11.84	11.87	15.03	11.80	12.52
Fe_2O_3	2.47	1.86	4.78	1.98	1.49
Mn O	0.03	0.02	0.07	0.02	0.07
Mg O	0.13	0.18	1.21	0.09	0.12
Ca O	0.48	0.58	2.62	0.44	0.47
Na_2O	3.36	3.30	3.51	3.57	3.59
K_2O	5.02	4.66	4.42	5.01	5.08
H_2O	0.55	0.51	0.85	0.44	0.63

(*) Supplied by Kleeman (1985) (Unpublished data).

Table 6-4.3 Trace element analysis of rock samples acquired from some tin mines in the study area. (Supplied by Kleeman (1985); Unpublished data).

	M1 351500 mE 6762000 mN	M2 367000 mE 6755500 mN	M3 367000 mE 6755500 mN	M4 375500 mE 6757000 mN	M5 372000 mE 6756500 mN	M6 366000 mE 6754000 mN	M7 372000 mE 6774000 mN	M8 370750 mE 6774500 mN
Fe	0.81	1.03	0.66	3.05	1.26	1.59	1.38	0.99
Sc	4.91	5.24	4.46	9.70	5.20	5.57	5.60	5.39
Cr	–	–	–	30.30	42.20	31.55	29.10	143.50
Co	(35)	(31)	(33)	5.	1.40	1.64	1.21	1.14
Zr	–	208.	235.	–	–	–	–	174.
Hf	4.73	5.66	5.37	6.70	5.1	6.52	5.63	5.94
Ta	(20)	(16)	(17.5)	–	2.53	2.61	3.73	3.53
Th	42.4	39.6	43.2	20.7	47.2	50.65	46.35	59.45
Na	2.43	2.22	2.36	2.32	2.26	2.19	2.3	2.4
K	–	–	–	3.5	2.95	–	4.45	–
Ba	193.	256.	251.	808.	189.	–	185.	–
Cs	17.9	26.	11.	20.4	30.35	31.4	17.45	13.2
Rb	437.	468.	493.	253.	563.	563.5	575.5	469.
La	30.47	40.5	30.	30.2	33.7	43.6	41.9	40.3
Ce	82.3	112.5	91.55	–	100.05	123.	116.	118.
Nd	55.7	70.7	55.6	–	43.8	–	–	67.2
Sm	11.3	11.3	14.2	7.22	13.3	13.7	12.8	15.2
Eu	0.29	0.3	–	1.06	0.24	–	–	–
Tb	1.43	2.23	1.92	0.75	1.75	2.26	1.85	2.14
Yb	8.91	8.93	10.7	2.55	9.25	12.45	10.12	13.7
Lu	1.6	1.68	2.07	0.72	1.75	2.31	2.08	2.4
U	18.7	17.3	25.6	6.56	17.8	19.85	16.6	17.5

(**) Data supplied by Kleeman (1985) (Unpublished data).

Note: 1). All of these may be artificially high in uranium concentration, because these locations are near tin mines.
2). All values have been normalized to standard rocks.

Chapter 7

DISCUSSION OF THE RESULTS

The airborne radiometric data

The airborne radiometric data analysed in this study were acquired at the same time as the magnetic data. An upward-looking detector was not used in the survey to monitor airborne radon. In addition, the spacing between flight lines was too wide to allow all detail to show up. A strip of at least 500 metre wide midway between flight lines would be essentially undetectable, radiometrically. The line spacing, combined with the distance between data stations posed problems in the gridding routine, because the tendency to produce patterns which is strongly influenced by the interpolation algorithm. Anisotropy in the maps would be undesirable since this obscures the data.

In addition, statistical adequacy was limited. For example, average raw counts for the uranium channel were 90 per station. Using the simple Poisson distribution, one relative standard deviation was 10%. The cumulative effect, after background removal, cosmic radiation subtraction, and spectral stripping, is for statistical scatter to become much greater.Therefore it would be unreasonable to attach excessive weight to a single reading (numbers of counts within a 0.8 second interval, over 50 metres flight distance). This was the major reason for using a moving-average, since the statistical scatter would be substantially reduced. One point to emphasize here is that, while I am grateful for the opportunity to use the data, it is must be recognized that it is reconnaissance data. There are definite limits to the amount of small-scale detail which can be expected from it.

In order to utilize airborne radiometrics for detailed scale work, it would be necessary to use more closely spaced flight lines, and if possible, to use upgraded equipment. The data acquisition system used in the survey was quite adequate, but an improvement in count rate would be necessary to achieve the statistical adequacy of every data point. It would also be very useful to evaluate the cost effectiveness of multiple detectors in order to reach higher count rates.

Radiometric signature of a tin mineralizing granite in the study area

The Mole Tableland area was chosen for detailed study because it includes the Mole Granite which has produced significant tin mineralization. The granite and the surrounding rocks have therefore been intensively studied geologically. Tin-mineralizing granites in New England, such as in this area, have distinct geochemical signature (Juniper and Kleeman, 1974) which includes high concentrations of U and Th (Kleeman, 1982) as well as moderate concentration of K.

Two types of maps which were produced in this study have, individually, different characteristics. These are maps of corrected and corrected-and-deconvoluted data of the airborne radiometric survey.

The maps of corrected data in many respects show patterns which are very similar to the geological map. Hence, these type of maps are useful for assisting geological mapping. However, it is unlikely that airborne radiometrics can entirely replace geological mapping, since a number of instances have been presented in which a distinction cannot be drawn between quite different rock types, such as sedimentary and igneous rocks. This was mainly because in those instances the concentrations of K, U, and Th are comparatively low, and are rendered unspecific by virtue of soil cover, weathering etc., so that it is not possible to make fine distinction between rock types where the signal is low and variable.

The maps of corrected-and-deconvoluted data of the airborne radiometric survey, on the other hand, enhance patterns of strong anomalies arising from the already-existing areas of mineralization associated with K, U, and Th. These maps can therefore be used as guidance for locating such areas with high potential of mineralization.

The data and the maps presented in previous Chapters show that the Mole Granite stands out prominently as a result of its geochemical signature. It is true that ground methods have, in the case of the Mole Granite, already discovered the tin mineralization, and outlined its particular chemical and petrological characteristics. The results from this study also show that granites with high U and Th abundance can be immediately and positively located. Such a granite would be recognized as prospective for tin and tungsten because of its high U and Th, and identified as a granite by its K abundance. Commonly, granites have 2.5 - 4 % K, but this could be ambiguous if used as the only diagnostic. Aerial photos or satellite imagery could be utilized as additional tools for distinguishing granites from surrounding rocks. The finding that the granite is geochemically specialized in U and Th would lead to further investigation by other more detailed exploration techniques.

Detection of sites of mineralization

Another reason of choosing the Mole Granite area was that it contains several styles of hard-rock mineralization (Weber, 1974). These can be classified into:

- deposits, mostly fracture-controlled type, which occur within the granite;

- mineralization, principally sheeted-vein style, in the country rock around the granite; and

- tungsten mineralization associated with silexite in the roof pendant (Lishmund, 1974; Weber, 1974; Kleeman, 1985).

The granite-hosted deposit occurrences mostly have distinct, albeit narrow, associated alteration zones, which are principally sericitic (Lonergan, 1971; Brett, 1972; and Brodie, 1983). Mineralization in the country rock is hosted by Permian Sediments (Stegman, 1983) or Permian Volcanics (Baillie, 1983) but originate from subsurface granite. The mineralization is accompanied by a variety of mineralogical and chemical changes. The silexite is also hosted by Permian Sediments in the roof pendant. This imprint is therefore potentially detectable by airborne radiometrics, because some of the alterations are potassic (Stegman, 1983; Baillie, 1983) and many also involve changes in U and Th.

In many respects, locations of the already-existing mineralization appear to overlap with patterns which represent high values of radiometric parameters on the coloured maps of corrected-and-deconvoluted data. This may be inspected by examining the coloured maps in Figures A6.12 - A6.17, with the map of the Mole Granite deposits provided for this purpose.

Detection of small bodies of contrasting lithologies

The results of the study also indicate that the method is capable of detecting comparatively small bodies of rocks. This is shown in the case of the I-type granite located 2 kilometres east of Torrington (376 500 mE; 6757 000 mN) and the Gibraltar Ignimbrite situated 5 kilometres to the north east of Silent Grove (369 000 mE; 6779 000 mN).

(i) The I-type granite east of Torrington

In this area, an exposed I-type granite of comparatively small dimensions (1.25 $\times$ 0.5 kilometres) clearly exhibit a low range of radiometric values in all maps presented in Figures A6.5 - A6.11. This can be attributed to an I-type granite which contrasts with the Mole Granite. Figures 7.1 and 7.2 show the location of the granite (Brett, 1972) and the eTh/K map of the particular area. Typical results of analysis of rocks acquired from this area are presented in Table 6-3.2.

In most cases, both the I-type granite and soil cover on the Mole Granite exhibit low values of TC, K, eU, eTh, eU/K and eU/eTh. However, the distinction between them is clear on the map of eTh/K parameter (Figure A6.11). In the area where the I-type granite exposed, the eTh/K parameter shows low values 1.5 - 6.0, whereas in the area on the Mole Granite with extensive soil cover, (378 500 mE; 6769 500 mN), this parameter exhibits high values 7.5 - 12.0. This can be explained as follows: During the chemical weathering process, thorium in resistate accessory minerals, especially monazite remains detritally in the alluvium and soil derived from granite, while a greater proportion of potassium is removed during rock weathering and erosion. This gives comparatively high values of eTh/K. Low values of eTh/K in the I-type granite are still under the influence of fresh rock.

(ii) The Gibraltar Ignimbrite

On all maps presented in Figures A6.5 - A6.11 this rock shows reasonably clear distinction from its surrounding sediments. However, exact borders between them cannot be drawn conclusively. This was mainly because insufficient radiometric contrast exists between those two rocks.

Distinctions amongst other rock types

The other rock types which include The Tent Hill Porphyrite, The Dundee Rhyodacite, The Permian Sediments, The Tertiary Basalt and the other granites in general do not show signature as distinct as the Mole Granite. In many respects the Permian Volcanics differ only slightly in radiometric values, from the Permian Sedimentary rocks. As a consequence, no sharp borders can be drawn between those two petrologically contrasting rock units. All of these rock units show comparatively low K, eU, and eTh. Moreover, soil cover attenuates the signal and adds a variable noise component to the point where it would be difficult to make fine distinctions.

The other granitoid plutons, which include an Undifferentiated Granite, The Clive Adamellite, The Pyes Creek Leuco-Adamellite, and The Bolivia Range Leuco-Adamellite are in general well delineated by medium to high values in radiometric parameters. This was mainly because they have sufficiently high radiometric values compared to the surrounding environment.

The Tertiary Basalt in the area shows low values of radiometric parameters, however, sharp borders between the basalt and the country rock cannot be drawn conclusively. This was also caused by insufficient radiometric contrast between those two rocks.

Factors effecting the intensity of radiometric signal

The signal reaching the γ-ray detector on board the aircraft is potentially modified by a number of factors at the source. These include:

(1) *soil cover to outcrop ratio;*

(2) *rock weathering;*

(3) *vegetation; and*

(4) *wetness of soil and rock.*

(1) Soil cover to outcrop ratio

During the experimental ground radiometric survey, this ratio was logged as percentage from 0% to 100%. Variation observed was from almost total soil cover to almost total outcrop. In some locations outcrop comprises huge whalebacks of comparatively unaltered granite in prominent ridges and bluffs.

One such area of almost total outcrop is in the region of the Curnows and Wallaroo mines (373 000 mE; 6754 000 mN). This area produced some of the highest values seen on the element maps. Another such area is located adjacent to Torrington-Silent Grove Road at 371 900 mE; 6762 200 mN. A very good reconciliation between airborne data and ground truth could be obtained for areas such as these. Table 7-1 lists the isolated data pairs of normalized count rate of the airborne radiometric and element concentration measured in the experimental ground radiometric survey. Average values for the Mole Granite are also shown (Kleeman, 1982; Enders, 1984).

It is possible that areas such as these may even give a slightly exaggerated airborne signal, because the outcrop is comprised of very large boulders and huge whalebacks on sharp ridges. In these cases, the signal could be enhanced because the effective source-to-detector distance could be somewhat less than the ground-to-air distance measured by radar altimeter and used for correction. However, this postulate is at present unsupported.

At the other end of the scale, there are areas almost completely covered by soil or alluvial cover. One area was described in Chapter 6, where a broad valley within the outcropping area of the Mole Granite (378 000 mE; 6769 500 mN) is occupied by granite-derived soil. The thickness of the soil is sufficient to absorb the gamma rays emitted from the bedrock. This area was traversed during the experimental ground radiometric survey and logged geologically and geomorphologically at the same time. Figures 7.3 and 7.4 show the potassium map and the topographic map of the area.

Potassium concentration of 1.0 - 2.0% characterized this area. Low concentration of this radiometric parameter may result from the removal of the potassium during the chemical weathering process. Notably, this area has a higher eTh/K ratio than the parent rock. This is because while potassium is removed, much of the thorium is retained in detrital monazite derived from the granite.

Normalized Count Rate			Concentration		
K (cps)	eU (cps)	eTh (cps)	K (pct)	eU (μg/g)	eTh (μg/g)
167.33	35.34	117.37	3.62	7.87	56.75
200.25	36.14	111.15	4.12	7.67	49.24
114.39	29.08	52.76	2.07	5.21	26.16
140.50	18.35	47.02	2.38	3.46	22.17
177.04	27.57	71.40	3.41	7.32	36.98
160.92	25.30	60.12	3.36	6.58	33.19
147.53	34.57	90.90	3.76	9.85	44.22

Table 7-1 Isolated data pairs of normalized airborne radiometric counts and radioelements concentrations measured in the experimental ground radiometric survey (The Silent Grove Road radiometric traverse).

(2) Rock weathering

Enders (1984) undertook laboratory gamma spectrometric analysis of equilibrated samples of weathered Mole Granite, and found a small depletion of eU and eTh. Enders (1984) also analysed K by conventional methods and measured an average concentration of 3.75%.

Guthrie and Kleeman (1986) show that a substantial proportion of the U in weathered granite is in alteration minerals in grain boundaries. Uranium daughter products in this form are easily out of equilibrium, since ^{222}Rn readily diffuses out, or is washed out by water penetration, leaving a resultant deficiency in ^{214}Bi. Notably, eU is much more reduced than eTh, as it is more prone to isotopic disequilibrium in this way. A diagnostic characteristic for rock weathering could be a substantially reduced eU/eTh ratio. Unfortunately, there are not enough areas of exposed deeply weathered granite to give consistent signal by airborne techniques to validate this method.

(3) Vegetation

Since the area is not covered by dense vegetation, this variable did not contribute to significant attenuation of the signal. This was confirmed during the experimental ground radiometric survey.

(4) Wetness of soil and rock

Water content retained by soil or rock may produce attenuation of the signal. Figure 7.5 shows radiometric profiles obtained before and after heavy rain, using the GAD-6/GSP-4 portable γ-ray spectrometer.

Considerable attenuation is produced, but it is difficult to quantify because of variation in attenuation with degrees of wetness. It is preferable that measurements are conducted under dry conditions. The airborne survey in this study was carried out in January-February 1982. The area was drought stricken and dry conditions prevailed. Furthermore there are no discontinuities visible in the data that would indicate heavy rainfall during the airborne survey.

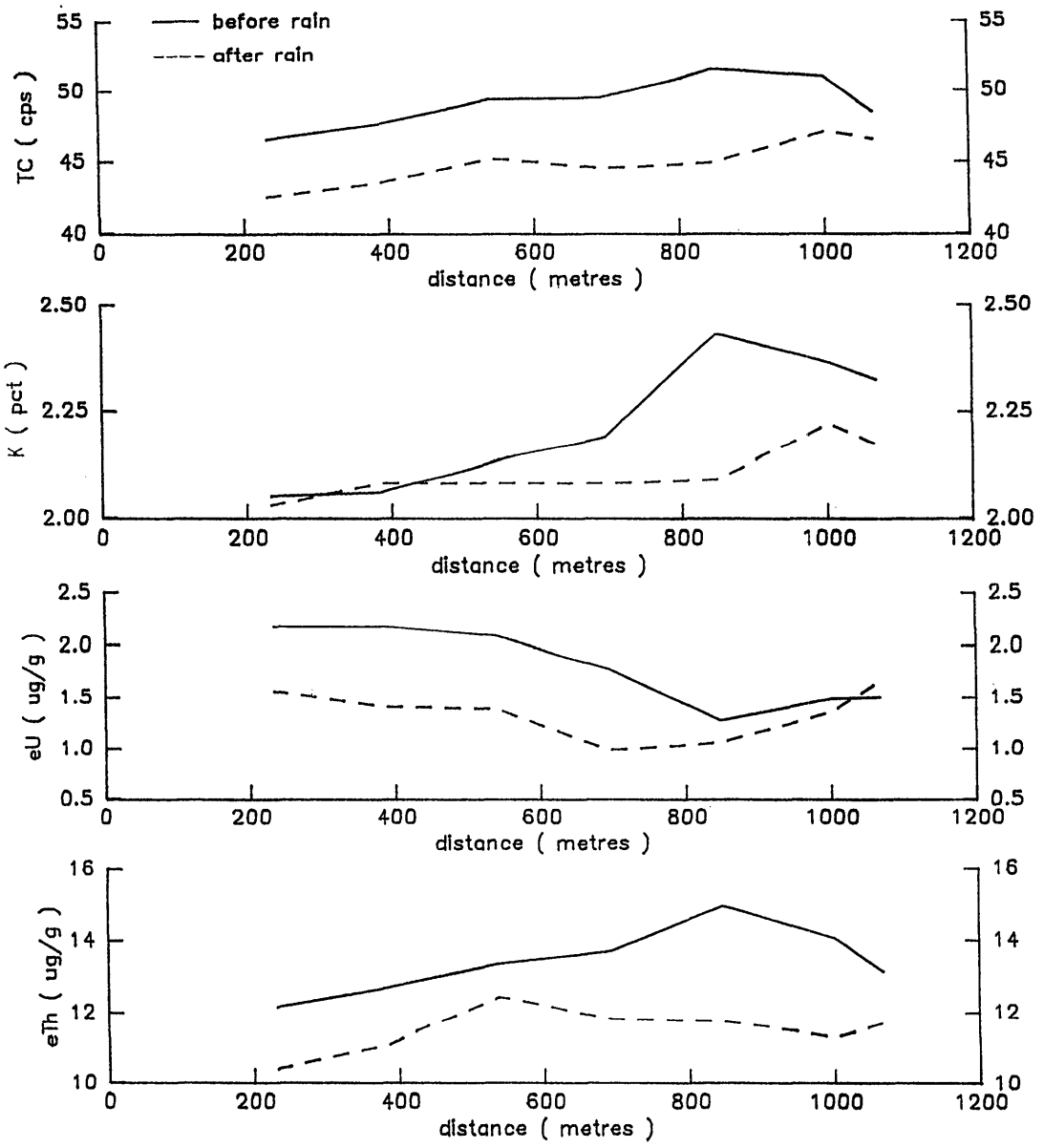

Figure 7.5 Radiometric profiles obtained before and after heavy rain.

Chapter 8

CONCLUDING REMARKS

This study has confirmed that the major medium scale control on the intensity of the radiometric signal is the soil-to-outcrop ratio. A portable γ-ray spectrometer was calibrated and carried on traverses, imitating the airborne data collection. This data reconciled with the airborne data, and there is high confidence in the calculations of K, eU, and eTh concentrations made from the airborne radiometric data. Areas with a very high proportion of exposed outcrop, yield values reasonably consistent with the actual abundance of the elements in the rocks studied.

Coloured maps of corrected data of total radiation count, K, eU, and eTh all give large scale patterns which outline the major geological units. Thus I conclude that airborne radiometrics are not only capable of outlining the distribution of certain large scale geological units, but will also yield credible calculated values of K, eU, and Th for suitable small areas within these subdivisions. Rock units with high values of K, U, and Th, and therefore with a strong signal, stand out prominently against units with low abundances. Granites are the most notable.

High heat production granites are commonly responsible for economic tin and/or tungsten mineralization as well as kaolinite. Radiometric methods are especially useful in locating these granites. Using total radiation count and K maps, most granites show up clearly in the coloured maps. The higher eU and eTh abundances discriminate between ordinary granites and those with the geochemical specialization necessary to produce mineralization. Thus areas warranting intensive study on a smaller scale can be identified.

Maps of corrected data were capable of locating a very small I-type granite of much lower radiometric signal within the Mole Granite. Areas of granite-derived alluvium and extensive soil cover can be recognized by their higher eTh/K ratios. However, it is often not possible to distinguish rock types with low radiometric signal because the low contrast is further depressed by the effect of variable soil cover.

The usefulness of the data on a small scale (areas of less than a square kilometre) is limited. An attempt was made to use the deconvolution technique to recover small areas of high signal intensity. The results of this are promising, but not altogether conclusive. While some good correlations were found with locations of known mineralization, some areas of known mineralization do not correlate with high values. A number of high anomalies which are not associated with known mineralization may warrant further investigation, by ground geological mapping and geochemical study.

A more detailed data set, with more closely spaced flight lines may be of use in detecting small radiometrically, anomalous areas associated with mineralization. This would vastly improved statistical adequacy with greater detector efficiency. A study of the cost effectiveness of larger, or multiple detector systems is considered worthwhile. Selected locations within this study area would be useful for such evaluation.